Department of Physics and Astronomy
University of Heidelberg

Bachelor Thesis in Physics
submitted by

Manuel Meske

born in Nürnberg (Germany)

2012

MC Simulation of Direct Photon HBT Correlations in Central Pb+Pb Collisions at $\sqrt{s}$ =2.76 TeV

This Bachelor Thesis has been carried out by Manuel Meske at the
Physikalisches Institut in Heidelberg
under the supervision of
PD Dr. Klaus Reygers

MC Simulation of Direct Photon HBT Correlations in Central Pb+Pb Collisions at $\sqrt{s}$ =2.76 TeV

Hanbury-Brown Twiss (HBT) interferometry is known to be a powerful tool to explore space-time dimensions of a Quark-Gluon Plasma created in heavy ion collisions. Experimental measurements of two-photon correlations at CERN SPS have been reported by the WA98 collaboration [1]. Within this thesis, the feasibility of a measuring HBT correlations of photons originated from a static thermal source with the ALICE detector at the LHC was studied. Since already existing HBT processors are not suitable for massless particles, an algorithm is presented that enables the simulation of photon pair correlations by making use of a new approach of detecting exactly one correlated photon pair per event applying the extracted experimental parameters. The significance of HBT correlations was estimated having regard to a huge background due to π^0 decay photons. By extracting the correlation strength, the fraction of direct photons was determined and compared to theoretical calculations. The influence of various detector and photon reconstruction constraints on the significance was analyzed by repeating the measurements with and without accounting for those effects.

MC Simulation von HBT Korrelationen direkter Photonen in zentralen Pb+Pb Kollisionen bei $\sqrt{s}$ =2.76 TeV

Hanbury-Brown Twiss (HBT) Interferometrie bietet eine mächtige Möglichkeit, Informationen über die Raum-Zeit Entwicklung des Quark-Gluonen Plasmas zu erhalten. Photon-Photon Korrelationen wurden bereits experimentell am CERN SPS Experiment von der WA98 Kollaboration gemessen [1]. Im Rahmen dieser Bachelorarbeit wurde die Machbarkeit einer Messung von HBT Korrelationen von Photonen, die nicht aus Hadron Zerfällen entstehen, mit dem ALICE Detektor am LHC untersucht. Da die bereits im verwendeten Analyse-Framework existierenden HBT Prozessoren für masselose Teilchen ungeeignet sind, wurde ein Algorithmus entwickelt, der die Simulation von Photon-Photon Korrelationen ermöglicht. Dabei wurde der Spezialfall betrachtet, dass genau ein Paar korrelierter direkter Photonen pro Event gemessen wird. Als Parameter für die Simulation wurden experimentelle Ergebnisse der WA98 Kollaboration verwendet. Die Signifikanz von HBT Korrelationen direkter Photonen wurde unter der Berücksichtigung des auftretenden hohen Untergrundes auf Grund von π^0 Zerfallsphotonen abgeschätzt. Durch Bestimmung der Korrelationsstärke wurde der Anteil direkter Photonen ermittelt und mit theoretischen Vorhersagen verglichen. Der Einfluss verschiedener Detektor- und Photon Rekonstruktions-Eigenschaften auf die Signifikanz wurde untersucht indem die Simulationen unter Berücksichtigung bzw. Nicht-Berücksichtigung dieser Effekte wiederholt wurde.

Contents

List of Figures

List of Tables

Chapter 1.

Introduction

The search for properties of the Quark-Gluon-Plasma (QGP), a deconfined phase of matter where quarks and gluons are free of their usual hadronic boundaries, stand among the most challenging as well as rewarding persuits of high energy nuclear physics today. Recent experiments at the Relativistic Heavy Ion Collider (RHIC) at Brookhaven and the Large Hadron Collider (LHC) at CERN give evidence to the existence of photons of low transverse momenta (p_T <3 GeV/c) which follow a thermal spectrum [6] and are not originated from hadronic decays. These observations shift the focus to even more interesting questions about the time evolution of the QGP.

It is expected that the quantum statistical correlations due to Hanbury Brown-Twiss (HBT) interference between these photons will provide valuable inputs for these investigations [12].
Theoretical investigations of the nature of photon correlations for relativistic heavy ion collisions where a QGP may be formed have been carried out by several authors [14, 15, 22]. Since photon interferometry in an experimental environment is faced with considerable difficulties due to the huge background of decay photons, so far only one measurement of direct-photon correlations in central Pb+Pb collisions has been reported by the WA98 collaboration at CERN SPS [1] at $\sqrt{s}$ =158 AGeV.
It is expected that such experiments will have higher possibility of success at LHC energies ($\sqrt{s}$ =2.76 TeV) where a larger initial temperature is expected. Moreover, with ALICE and its Time Projection Chamber (TPC) and Inner Tracking System (ITS) a heavy ion experiment is available that provides a unique momentum resolution especially for low transverse momenta [10].

This thesis presents a feasibility study for a measurement of photon-photon correlations with the ALICE detector. The significance of a two-photon HBT signal is estimated in the invariant mass spectrum of $\pi^0 \rightarrow \gamma\gamma$ decays which are the primary source of decay photons with a typically amount of $\cong$ 90% [8]. The HBT processors that are already existing in the used analysis framework only work for charged particles and particles with mass. Thereby a new algorithm has been developed that is able to simulate HBT correlations of photon pairs under the assumption of the special case that exactly one correlated photon pair is detected per event.

After the theoretical background of the QGP, direct photons and HBT interferometry are explained briefly, the developed algorithm is described step-by-step in a detailed manner.
In order to illustrate the MC simulation, direct photon HBT correlations are first analyzed without adding any decay photons. Thus, the input parameters of the simulation can be obtained that reproduce correlation functions which are similar to the ones extracted in the WA98 experiment.
Neutral π^0 decays are added to the simulation to study the influence of a huge background due to decay photons on the obtained correlation function. In order to simulate an experimental setup, various detector- and photon reconstruction constraints are implemented step-by-step. Thereby the impact of these constraints on the significance of the HBT signal can be investigated.

Chapter 2.

Theoretical Background

2.1. The Quark-Gluon-Plasma

High energy physics describes the strong force in terms of elementary particles (quarks) interacting through the exchange of gauge bosons (gluons). The asymptotic freedom states that the effective coupling constant of Quantum Chromodynamics (QCD) falls with increasing momentum transfer q^2. In a thermal medium, the characteristic momentum transfer between particles is of the order of the temperature. Under low temperature conditions, quarks are confined in hadrons. Increasing the temperature or baryon density would cause nuclei to deconfine and a hadron gas is formed. After further heating or compressing, this hadron gas melts down to a strong interacting system of quarks and gluons, the Quark-Gluon-Plasma (QGP).

It is believed that such a phase of matter has been existed in the early stage of our universe until 10^{-5} s after the Big Bang [16]. Today, deconfined matter only exists in neutron stars, super novae or artificially created in the laboratory. The best opportunity for recreating the conditions of a QGP is provided by relativistic nucleus-nucleus collisions such as Au+Au or Pb+Pb collisions. Such experiments have already been performed at SPS [4] and RHIC [5].

2.2. Direct Photons

In relativistic heavy-ion collisions direct photons is used to mean photons not originated from hadron decays. Observing direct radiation from a QGP state has been a central part of the motivation to measure photon production in relativistic heavy-ion collisions. Direct photons are created throughout the whole lifetime of a heavy-ion collision, so that the measurement of them mainly serves two interests [8]:

- the study of *prompt photon* production to learn about hard processes in the dense QGP medium

- the understanding of the thermal properties of the early phase of the reaction from *thermal photons*

While their identification is very difficult, especially at low transverse momenta, because of the huge background from decay photons, direct photons do not interact strong, thus they provide unique and unperturbated information on the earliest stages of the collision. In the low p_T domain (p_T <3 GeV/c), the thermal photons dominate the spectrum. There are several sources of thermal photons, including the early radiation from the equilibrated QGP or the later radiation of the hot hadron gas [8].

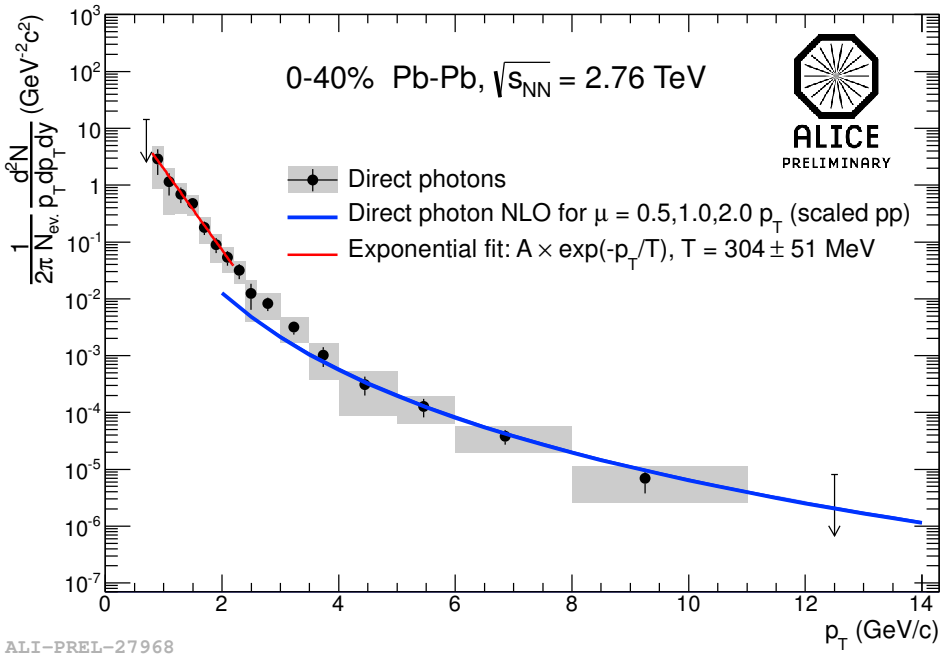

Figure 2.1.: Direct Photon Spectrum [9] for the $0-40\%$ most central events. For investigating thermal photons with transverse momenta p_T <3 GeV/c the exponential fit will be extrapolated towards lower p_T.

As shown in Figure 2.1 the low p_T (p_T <3 GeV/c) domain of the spectrum of the $0-40\%$ most central events can be described by a thermal spectrum:

$$\frac{1}{2\pi N_{ev.}} \frac{d^2N}{p_T dp_T dy} \propto \exp\left(-\frac{p_T}{T}\right) \tag{2.1}$$

where y is the rapidity and $N_{ev.}$ is the total number of measured events. The temperature in this kinematic range can be extracted from the fit to $T = (0.304 \pm 0.051)$ GeV/c.
As this analysis investigates direct photons with transverse momenta p_T <3 GeV/c, this fit function will be extrapolated towards lower p_T and used for generating thermal photons in a MC simulation. Since the simulation has been performed before the above preliminary plot was published, a slope of T =0.266 GeV/c has been used instead. This

parameter is substantially larger than the temperature obtained in central Au+Au at $\sqrt{s}$ =200 GeV collisions at PHENIX where the slope of the thermal spectrum has been extracted to $T = (0.220 \pm 0.020)$ GeV/c [6, 7]. In the case of central Pb+Pb collisions at $\sqrt{s}$ =2.76 TeV a much higher temperature is expected. Which is why a parameter of T =0.266 GeV/c was chosen. According to Figure 2.1 this guess agrees within 1σ with the obtained temperature of $T = (0.304 \pm 0.051)$ GeV/c so that the p_T spectrum used in the MC simulation of this analysis describes the observed one to a reasonable accuracy.

Chapter 3.

Hanbury Brown-Twiss (HBT) Interferometry

Historically Hanbury Brown-Twiss (HBT) interferometry was proposed and developed by Hanbury-Brown and Twiss in the 1950's as a method to determine the dimension of distant astronomical objects. They applied the method to a measurement of the angular diameter of the star Sirius [23]. A few years later, the same technique has been to pion pairs emitted from proton-anti proton collisions [25].
By then HBT interferometry is known to be a powerful tool to explore space-time dimensions of the hot zone created in heavy ion collisions. It is expected that the quantum statistical interference between emitted identical particles will provide valuable inputs for these investigations [20, 35].
Since these hadronic correlations reflect the space-time dimensions of the source at freeze-out time, further complementary information can be obtained from direct photon-photon correlations. Photons are assumed to be emitted mostly from the central hot zone and reflect the history of the hottest part of the collision.
There are some further advantages of using photons for such studies. They are free from distorting effects like the re-scattering and Coulomb interaction. Therefore, HBT parameters can be measured in the photon channel with smaller systematic errors [14].
Unfortunately, photon interferometry is faced with considerable difficulties due to the small fraction of direct photons in comparison to the huge background of photons produced in meson decays (particularly $\pi^0 \to \gamma\gamma$ and $\eta \to \gamma\gamma$).
The following sections present some basics of HBT interferometry, before both a one- and three-dimensional parametrization of the two-photon correlation function are discussed.

3.1. Basics of Intensity Interferometry

Intensity interferometry compares, in contrast to *amplitude* interferometry, the intensity of two or more particle wave functions. While amplitude interferometry can only be used

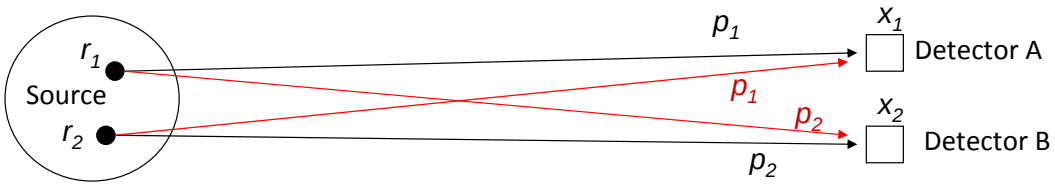

Figure 3.1.: Setup of an HBT intensity interferometry experiment. Since we cannot distinguish between the two situations (black and red) both amplitudes have to be added.

for coherent sources, HBT is only meaningful with an incoherent source.

The following derivations should give a brief introduction into the theoretical formalism of HBT correlations in high energy physics. A very detailed theoretical review can be found in [12].
Consider a source with a density function $\rho(r)$, emitting two identical particles at space-time points r_1 and r_2, as shown in Figure 3.1. Their four momenta p_1 and p_2 are measured by some detectors at points A and B.
The HBT effect means that a correlation function C_2 defined as

$$C_2(p_1, p_2) = \frac{P(p_1, p_2)}{P(p_1) \cdot P(p_2)} \tag{3.1}$$

is greater than unity for some values of p_1 and p_2. $P(p_1, p_2)$ and $P(p_{1,2})$ are the two- and one-particle probabilities of observing events with particles of specific momenta. Suppose also that a particle with momentum p_i is detected at the space-time point x_i. In order to receive a more detailed description of this scenario we have to make the following assumptions:

- The emission of both particles is uncorrelated, i.e., that the two-particle space-time distribution of the emitting source $\rho(r_1, r_2)$ can be written as the product of the single-particle emissions, $\rho(r_1, r_2) = \rho(r_1)\rho(r_2)$.
- The emitted particles propagate as free particles after their emission, i.e., that they can be represented by plane waves [22]:

  $$\Psi_i(p_i) = N(p_i) \cdot e^{ip_i(x_i - r_i)} \tag{3.2}$$

  where $N(p)$ is a normalization constant only dependent on p and r_i is the production point of the particle.

These assumptions allow us to write

$$P(p_1, p_2) = \int |\Psi_{12}(r_1, r_2; x_1, x_2)|^2 \cdot \rho(r_1)\rho(r_2) d^4r_1 d^4r_2 \tag{3.3}$$

with the two-particle wave function:

$$\Psi_{12}(r_1, r_2; x_1, x_2) = \frac{1}{\sqrt{2}} \left[e^{ip_1(x_1-r_1)} e^{ip_2(x_2-r_2)} + e^{ip_1(x_1-r_2)} e^{ip_2(x_2-r_1)} \right] \tag{3.4}$$

To get the two-particle correlation function C_2 one has to define the denominator of equation 3.1. The single particle distributions $P(p_i)$ are given by:

$$P(p_i) = \int |\Psi_i(r_i; x_i)|^2 \cdot \rho(r_i) d^4 r_i \tag{3.5}$$

with the wave function $\Psi_i(r_i; x_i)$ defined in equation 3.2.
The correlation function C_2 is then given by the following expression:

$$C_2(p_1, p_2) = C_2(q) = 1 + |F_{12}|^2 \tag{3.6}$$

where

$$|F_{12}| = \int d^4 x \rho(x) e^{iqx}; \qquad q = p_1 - p_2 \tag{3.7}$$

Here, q is the momentum difference of the two particles, also called the relative momentum.
As a consequence of the symmetric assumption in the wave function of equation 3.4, identical bosons favor small relative momenta q compared to nonidentical particles. The measurement of the correlation function C_2 provides insight to the (single-particle) emitting source function $\rho(r)$ through its Fourier-transform. One usually assumes the shape of $\rho(r)$ and checks this against experimental data [14].
Since various experiments showed that $C_2(q = 0)$ is considerably smaller than 2 [22], equation 3.6 has been modified by introducing the so called *correlation strength* $\lambda \in (0, 1)$, which gives the fraction of pairs of identical particles which appear to interfere.
After introducing this parameter, the correlation function can be written as

$$C_2(p_1, p_2) = C_2(q) = 1 + \lambda \cdot |F_{12}|^2 \tag{3.8}$$

If we consider two emitted photons, we have to take into account the spin of the photons. It was shown in [15] that an accurate treatment of the current conservation relations leads to the following expression for the correlation strength for photons:

$$\lambda = \frac{1}{2} \tag{3.9}$$

The correlation strength λ equals 1/2 for a fully chaotic source and 0 for a fully coherent source.
This expression has lead to discussions for years, but since $C_2(q)$ is a Lorentz scalar and it is impossible to construct a dimensionless Lorentz scalar from two massless four-vectors, λ can only be a constant [14].

Under the assumption of a fully chaotic photon source, λ is a measure of thermal photons N_γ^{Direct} vs. the total inclusive photon yield $N_\gamma^{Total} = N_\gamma^{Direct} + N_\gamma^{Decay}$ [1, 18], where the decay photons are assumed to be emitted mostly from neutral $\pi^0 \to \gamma\gamma$ decays.
The ratio of the obtained correlation strength λ and the assumed correlation strength $\lambda_{in} = 1/2$ of the fully chaotic thermal photons is given by:

$$\sqrt{\frac{\lambda}{\lambda_{in}}} = \sqrt{2\lambda} = \frac{N_\gamma^{Direct}}{N_\gamma^{Direct} + N_\gamma^{Decay}} = \frac{N_\gamma^{Direct}}{N_\gamma^{Total}} \tag{3.10}$$

By measuring the total photon yield N_γ^{Total} one can obtain the fraction of direct photons from the intercept of C_2 on the y-axis [1].

3.2. Parametrization of the Correlation Function for Direct Photons

Equation 3.8 states a very general formulation of the correlation function. Assuming that the original source density distribution $\rho(r)$ is a Gaussian distribution, its Fourier transform will also be a Gaussian, thus the correlation function will form a Gaussian distribution, too [31].

3.2.1. Three-Dimensional Parametrization

The results for the correlation function $C_2(q)$ are best discussed by using so called "out-side-long" coordinates, also known as "Bertsch-Pratt" coordinates. As shown in Figure 3.2, the relative three-momentum of both photons $\vec{q} = \vec{p_1} - \vec{p_2}$ gets decomposed into outward (q_{out}), sideward (q_{side}) and longitudinal (q_{long}) components.
In order to transform the coordinate system it is suitable to introduce the average three momentum k of both photons:

$$\vec{k} = \frac{1}{2}(\vec{p_1} + \vec{p_2}) \tag{3.11}$$

The "out" component q_{out} is the projection of $\vec{q}$ onto the direction of the pair transverse momentum $(\vec{p_{T_1}} + \vec{p_{T_2}})$. q_{long} is the component of $\vec{q}$ along the beam direction and q_{side} is the projection of the relative momentum onto the third perpendicular direction.

After defining the difference and the average of the transverse momenta p_{T_1} and p_{T_2},

$$\vec{q_T} = \vec{p_{T_1}} - \vec{p_{T_2}} \qquad \vec{k_T} = \frac{1}{2}(\vec{p_{T_1}} + \vec{p_{T_2}}) \tag{3.12}$$

we can transform [36, 37] the components of $\vec{q}$.
The reference frame most commonly used for this purpose is the so called Longitudinal Co-Moving System (LCMS), where the longitudinal momentum of the pair vanishes:

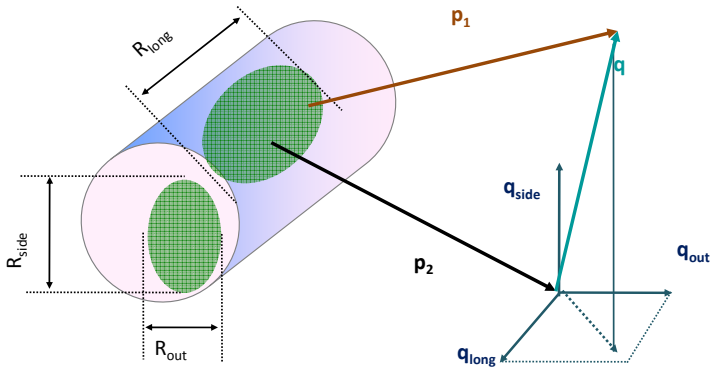

Figure 3.2.: In the Longitudinal Co-Moving System (LCMS) the relative momentum $\vec{q}$ gets decomposed into outward, sideward and longitudinal coordinates [18]. The

$$p_{z_1}^{LCMS} + p_{z_2}^{LCMS} = 0 \tag{3.13}$$

The conversion between the lab frame and the LCMS frame can be done as follows [38]. First one needs the necessary longitudinal velocity of the LCMS frame so that relation 3.13 holds:

$$\beta_z = \frac{p_{z_1} + p_{z_2}}{|\vec{p_1}| + |\vec{p_2}|} \tag{3.14}$$

Now the momenta of each photon in the lab frame are boosted by β_z:

$$p_x^{LCMS} = p_x; \qquad p_y^{LCMS} = p_y \tag{3.15}$$

$$p_z^{LCMS} = \gamma_z \cdot (p_z - \beta_z \cdot \vec{p}); \qquad \gamma_z = \frac{1}{\sqrt{1-\beta_z^2}} \tag{3.16}$$

The three coordinates of the relative momentum $\vec{q}$ can now be calculated by:

$$q_{out} = \frac{\vec{q_T} \cdot \vec{k_T}}{\left|\vec{k_T}\right|} \tag{3.17}$$

$$q_{side} = \frac{|\vec{p_{T_1}} \times \vec{p_{T_2}}|}{\left|\vec{k_T}\right|} \tag{3.18}$$

$$q_{long} = p_{z_1}^{LCMS} - p_{z_2}^{LCMS} \tag{3.19}$$

In this coordinate system, the correlation function $C_2(q)$ can be approximated [36] by:

$$C_2(q_{out}, q_{side}, q_{long}) = 1 + \lambda \cdot \exp\left[-\left(q_{out}^2 R_{out}^2 + q_{side}^2 R_{side}^2 + q_{long}^2 R_{long}^2\right)\right] \tag{3.20}$$

where the HBT radii parameters R_{out}, R_{side} and R_{long} provide information about the size of the extending system. In the language of Sinyukov [29] this size can be termed as the "region of homogeneity", i.e. the region from which particle pairs with momentum p are most likely emitted.

3.2.2. One-Dimensional Parametrization

Since measuring the HBT correlations using a three-dimensional parametrization requires very high statistics, from the experimental point of view it is much easier to extract the source distribution over the invariant relative momentum $q_{inv} = \sqrt{-q^2}$.
A one-dimensional correlation function for photons can be constructed by [14]:

$$C_2(q_{inv}) = 1 + \lambda \cdot e^{-R_{inv}^2 q_{inv}^2} \tag{3.21}$$

where

$$\begin{aligned} q_{inv} &= \sqrt{-(p_1^\mu - p_2^\mu)^2} = \sqrt{(\vec{p_1} - \vec{p_2})^2 - (|\vec{p_1}| - |\vec{p_2}|)^2} \\ &= \sqrt{2\,|\vec{p_1}|\,|\vec{p_2}|\,(1 - \cos\theta)} \end{aligned} \tag{3.22}$$

In the case of massless particles q_{inv} is equal to the pair invariant mass $m_{\gamma\gamma}$. Therefore the one-dimensional measurement of the correlation function $C_2(q_{inv})$ can be used to estimate the significance of two-photon correlations in the invariant mass spectrum.

Figure 3.3 shows some exemplary plots of $C_2(q_{inv})$, where R_{inv} and λ are varied.
However, the corresponding radius R_{inv} contains only averaged information about the space-time dimensions. The actual two-photon correlation function C_2 is decided by

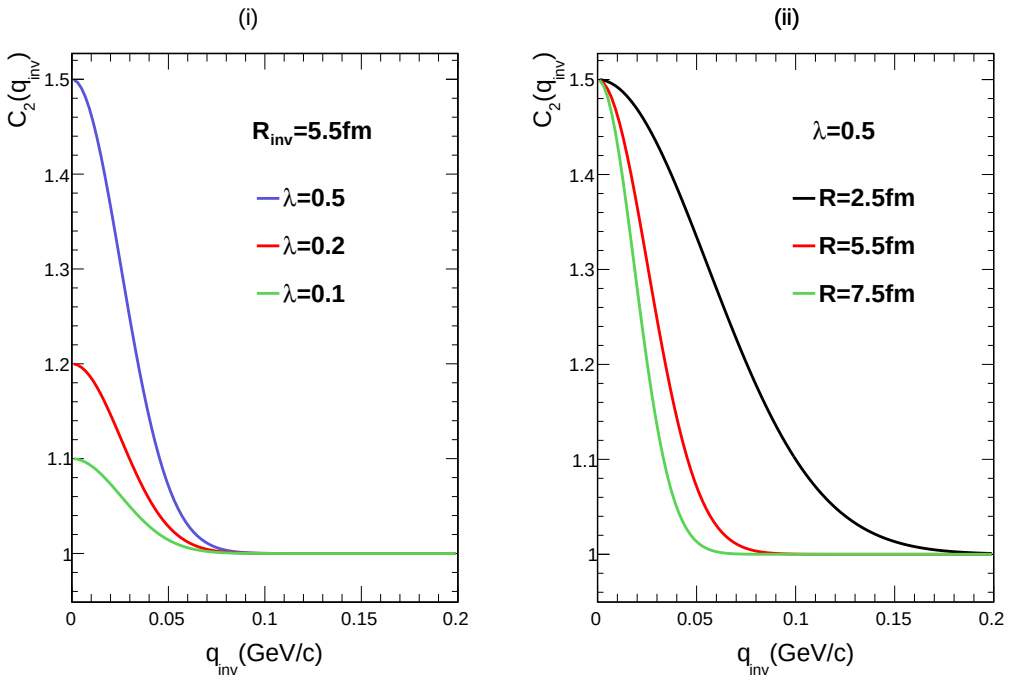

Figure 3.3.: The One-dimensional two-photon correlation function $C_2(q_{inv})$.(i) The correlation strength λ can be obtained from the intercept on the y-axis.(ii) As the radius grows, the width of the distribution gets smaller.

the range of the outward, sideward and longitudinal components of the momentum difference. As even a given value of q_{inv} will only provide a range of these momentum-differences, the one-dimensional correlation function will be obtained by taking an average over the corresponding three-dimensional results. This will lead to an effective λ which will not rise to 0.5, even if there were no decay photons.

3.3. Results of the WA98 Experiment at CERN

So far, the only experiment, which measured correlations of photons originated from hadronic reactions and possibly quark matter, has been reported by the WA98 Collaboration for central ^{208}Pb+^{208}Pb collisions at $\sqrt{s} = 158$ AGeV. The analysis presented in [1] was performed on the 10% most central collisions with a total sample of 5.8×10^6 events.

As shown in Figure 3.4, the correlation function was calculated both for $0.1/c < k_T < 0.2$ GeV/c and $0.2/c < k_T < 0.3$ GeV/c as the ratio of the distribution of photon pair invariant relative momenta q_{inv}. k_T indicates the magnitude of $\vec{k_T}$. As it is typically done in experimental constructions of the correlation function, the correlated numerator of eq.

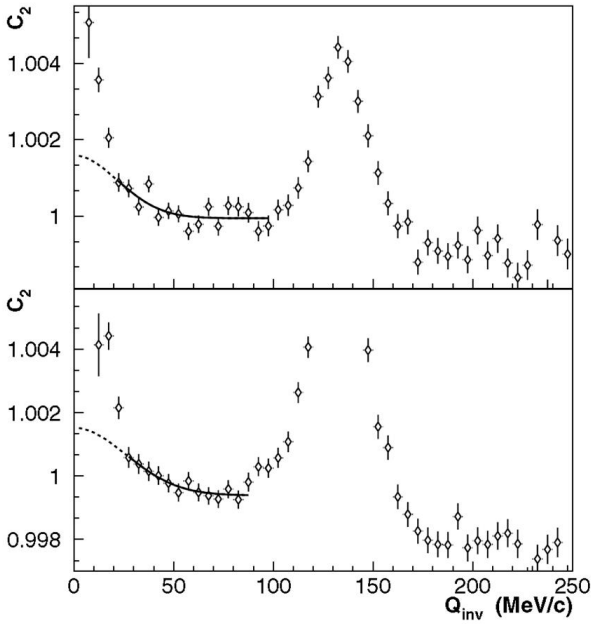

Figure 3.4.: The two-photon correlation function for average momenta $0.1 < k_T < 0.2$ GeV/c and $0.2 < k_T < 0.3$ GeV/c. The solid line shows the fit in the fit region used and the dotted line shows the extrapolation into the low q_{inv} region where backgrounds are large [1].

3.1 has been taken from photons from the same event. The denominator is used to be the uncorrelated background distribution which is built by constructing pairs of photons taken from different events (*event mixing* technique). The ratio was normalized to get an equal number of photon pairs in the numerator and denominator.
The correlation function then has been fit with a one-dimensional Gaussian parametrization, as it is described in 3.2.2 and the invariant interferometric radii and correlation strengths were extracted. The fit region does not include the very low q_{inv} region, where the rise of the correlation function is assumed to be superimposed by single hadron or photon showers that are split into nearby clusters (*cluster splitting*) [1].
The following HBT parameters were obtained:

k_T range	λ	R_{inv} [fm]
(1)	0.0028 ± 0.0004(stat.)± 0.0006(syst.)	5.4 ± 0.8(stat.)± 0.9(syst.)
(2)	0.0029 ± 0.0007(stat.)± 0.0016(syst.)	5.8 ± 0.8(stat.)± 1.2(syst.)

Table 3.1.: HBT correlation parameters for direct photons obtained by the WA98 collaboration for average momenta (1) $0.1 < k_T < 0.2$ GeV/c and (2) $0.2 < k_T < 0.3$ GeV/c

The invariant interferometric radii R_{inv} were found to be similar to the ones obtained in former π^- correlation studies. This suggests that the direct photons of this k_T region

are emitted in the late, hadron gas, stage of the ^{208}Pb $+^{208}$ Pb collision.
Furthermore the correlation strength was used to extract the yield of direct photons for k_T <0.3 GeV/c. By applying equation 3.10 the ratio of direct photons to the total number of photons was calculated to $N_\gamma^{Direct}/N_\gamma^{Total} \cong 10\%$.
In ALICE a rate of $N_\gamma^{Direct}/N_\gamma^{Total} \cong 5-10\%$ is assumed, thus a HBT analysis of direct photons is expected to provide correlation strengths of the same magnitude.

Chapter 4.

MC Simulation of Direct Photon HBT Correlations

The following sections present a Monte Carlo method to simulate thermal Photons correlations in `AliRoot`.
After a thorough description of the implemented algorithm, the significance of direct photons is extracted when π^0 decay photons are added. The obtained results are compared to the ones from the WA98 experiment, listed in Table 3.1

4.1. Simulating Direct Photon HBT Correlations

As there is no HBT processor for direct photons yet implemented in the used analysis framework (`AliRoot`), the first task was to develop a Monte Carlo simulator, which adds photon-photon correlations to a given event generator.
The already existing and fully implemented `AliGenHBTProcessor` class only works for charged particles and particles with mass, but no reasonable results were obtained when trying to use the routine for photons. The method that is used in this generator is based on random shifts of the particle three-momentum [40]. After each shift, a comparison is made with the correlation function. The shift is kept if the χ^2-test shows better agreement. This process is iterated until satisfactory agreement is achieved.
Since this algorithm is very complex and suffers a long runtime it is not suitable to adopt it for direct photon-photon HBT correlations.
Instead, a simpler method was designed that makes use of the following assumptions to provide a rough estimate of the significance of photon correlations:

- All photons are generated according to a static thermal photon source.
- The simulation treats the **special case** that exactly two direct photons are emitted and detected each event.
- Besides the photon correlations no correlations of other particles (e.g. π) are contributing to the simulation.

4.1.1. Description of the implemented Algorithm

The developed algorithm of simulating photon-photon correlations according to a given two-photon correlation function C_2 employs the three-dimensional parametrization described in section 3.2.1.
The main idea is to generate one direct photon γ_1 which fulfills the transverse momentum p_T, pseudo-rapidity η and azimuthal angle ϕ conditions for thermal photons. The second photon then gets calculated on the basis of γ_1 and a randomly picked $(q_{out}, q_{side}, q_{long})$ set, which follows a distribution defined by the given three-dimensional correlation function $C_2(q_{out}, q_{side}, q_{long})$.
The flow diagram shown in Figure 4.1 gives a rough overview of the single steps of the simulation, which are presented hereafter in detail.
The simulation is divided into two main parts where the first part (red boxes) is responsible for the generation of a distribution of $\vec{q}$ where the $(q_{out}, q_{side}, q_{long})$ set is picked from. For this purpose the simulation makes use of coarse background histogram.
The second part (blue boxes) covers the actual generation of the HBT signal. Both the final signal and background histograms are filled for different k_T bins and the single components of $\vec{q}$ can be projected.

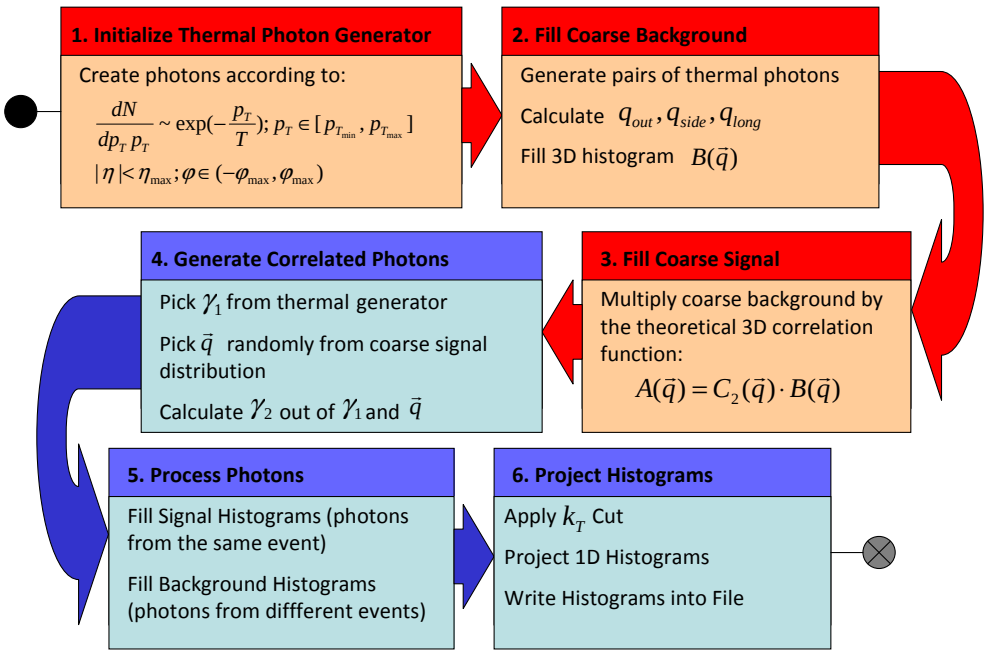

Figure 4.1.: Flow diagram of the direct photon HBT simulation making use of the three-dimensional parametrization of the two-photon correlation function $C_2(\vec{q})$.

1. Initialize Thermal Photon Generator:

The thermal photons are generated from a simple photon generator, which randomizes the transverse momentum p_T, the pseudo rapidity η and the azimuthal angle ϕ out of the following distributions:

$$p_T : \frac{dN}{dp_T p_T} \propto \exp\left(-\frac{p_T}{T}\right), \qquad p_T \in [p_{T_{min}}, p_{T_{max}}]$$
$$\eta : \text{Uniformly distributed between } (-\eta_{max}, \eta_{max}), \eta_{max} = 0.9$$
$$\phi : \text{Uniformly distributed between } (-\pi, \pi)$$

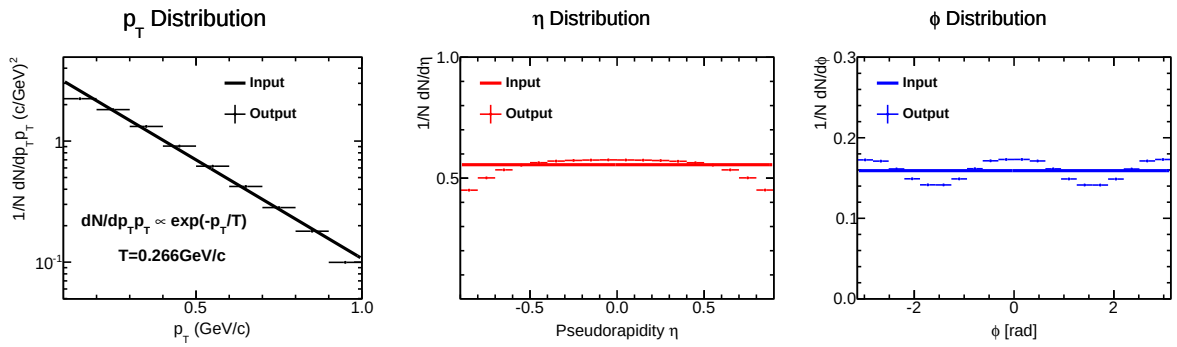

Figure 4.2.: The simulated spectra slightly differ from the input distributions which are indicated by the solid lines. The data points are provided by an exemplary simulation of direct photons originated by the above generator in $N_{ev.} = 2 \times 10^7$ events. The distributions were normalized by the total number of events and the corresponding bin width.

Figure 4.2 shows the input (solid lines) and output distributions of p_T, η and ϕ, where photons with a kinematic window of $p_T \in [0.1, 1.0]$ GeV/c, $|\eta| < 0.9$ and $\phi \in (-\pi, \pi)$ are generated. The single distributions were normalized by the number of events and the corresponding bin width.
The p_T spectrum most closely corresponds to the thermal spectrum that was put in. The extracted temperature T of a fit in the low p_T domain matches the input parameter quite well (T =0.266 GeV/c).
The occurring deviations for $\eta > 0.7$ and ϕ are resulting from the two-photon correlations.

2. Fill Coarse Background:

A coarse background histogram is generated from the photons given by the thermal photon generator. After two photons with four-momenta p_1 and p_2 are generated, the

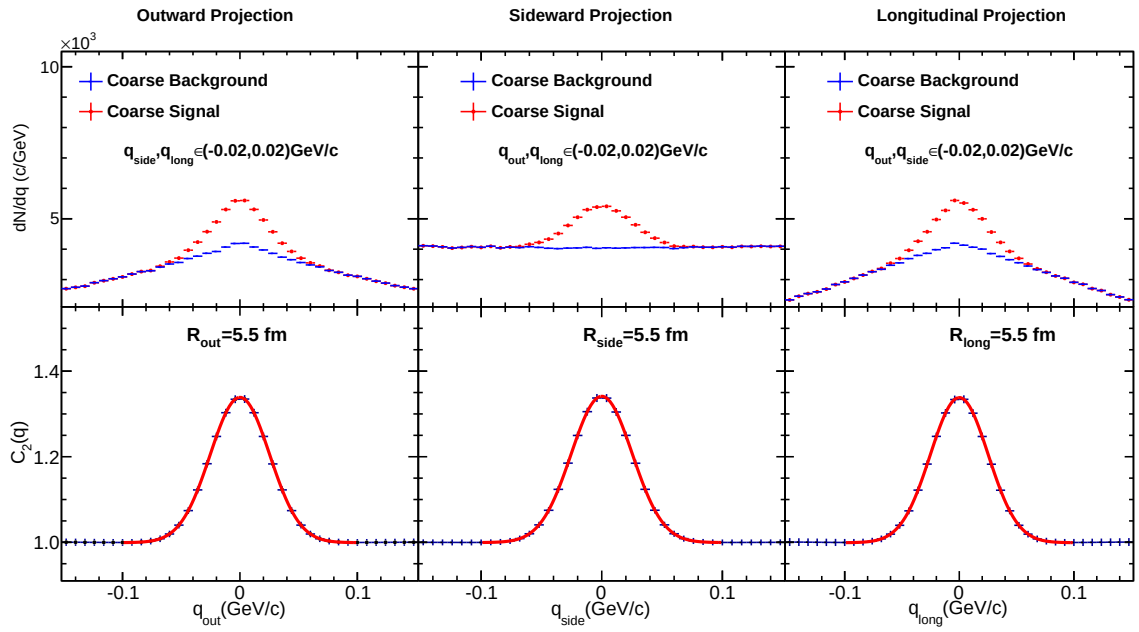

Figure 4.3.: One-dimensional projections of q_{out}, q_{side} and q_{long} of the three-dimensional coarse signal and coarse background histogram together with the corresponding correlation functions $C_2(q_i)$. $C_2(q_i)$ are obtained by division of the correlated spectra (red markers) by the uncorrelated spectra (blue markers).

relative momentum $\vec{q} = (q_{out}, q_{side}, q_{long})$ gets calculated as presented in eq. 3.17-3.19 and filled into a three-dimensional coarse background histogram $B(\vec{q})$.

3. Fill Coarse Signal:

Once the coarse background is filled with a suitable number of entries to guarantee appropriate statistics, the coarse signal histogram $A(\vec{q})$ is produced by multiplying the coarse background bin by bin by the required three-dimensional two-photon correlation function:

$$\begin{aligned} A(\vec{q}) &= C_2(\vec{q}) \cdot B(\vec{q}) \\ C_2(\vec{q}) &= C_2(q_{out}, q_{side}, q_{long}) = \\ &= 1 + \lambda \cdot \exp\left[-\left(q_{out}^2 R_{out}^2 + q_{side}^2 R_{side}^2 + q_{long}^2 R_{long}^2\right)\right] \end{aligned} \tag{4.1}$$

Figure 4.3 shows the one-dimensional projections of the three-dimensional coarse background and coarse signal histograms together with the corresponding projections of the correlation function $C_2(\vec{q})$. The sample is multiplied by a correlation function where the

radii are $R_{out} = R_{side} = R_{long}$ =5.5 fm. When projecting on one axis, the other two components were required to be within (-0.02,0.02) GeV/c.

4. Generate correlated Photons:

The actual HBT signal can now be produced by randomizing out of the coarse signal distribution. While the first photon γ_1 with four-momentum p_1 is taken from the thermal photon generator in (1.), the four momentum p_2 of the second photon γ_2 gets calculated on the basis of the first one and a relative momentum $\vec{q} = (q_{out}, q_{side}, q_{long})$ that is picked randomly out of the coarse signal distribution.
For this calculation a numerical method included in the `AliRoot` class `AliGenHBTosl` is applied.

5. Process Photons:

While the final three-dimensional signal histogram is filled by calculating the relative momenta $\vec{q}$ according to equations 3.17-3.19 for each photon pair taken from the same event, the background histogram is produced by taking both photons from different events.
Besides filling the three-dimensional histograms, both the invariant relative momentum q_{inv} (eq. 3.22) and the average transverse momentum k_T (eq. 3.12) are computed out of the four momenta p_1 and p_2 of the two generated photons γ_1 and γ_2.
If one is only interested in entries within a given k_T-range, the signal and background histograms are filled after a cut in k_T.

6. Project Histograms:

The one-dimensional distributions of the relative momentum components $q_{out}, q_{side}, q_{long}$ are obtained by projecting the three-dimensional signal and background histograms.

When projecting on one axis q_i the other two components $q_{j,k}$ $(i, j, k \in \{out, side, long\})$ are required to be within a given momentum range $[-\frac{\Delta q_{j,k}}{2}; \frac{\Delta q_{j,k}}{2}]$, where $\Delta q_{j,k}$ will now be termed as *projection width*. The entries of the projection then get integrated over this range.
The one-dimensional projections and their correlation functions are illustrated in Figure **??**, where an exemplary simulation of 2×10^7 events is analyzed within a k_T window of $k_T \in (0.2, 0.3)$ GeV/c. The one-dimensional two-photon correlation function is calculated by dividing the projection of the correlated signal histogram (red markers) by the uncorrelated background histogram (blue markers).
Additionally the q_{inv} histogram and its corresponding correlation function $C_2(q_{inv})$ are illustrated on the right hand side.

4.1.2. Analysis of the Coarse Signal

Before we start to simulate HBT photons it is reasonable to have a look at the method which provides us with the one-dimensional projections of the three components of the relative momentum $\vec{q}$. Here it is suitable to investigate the generated three-dimensional coarse signal histogram because the correlation functions $C_2(q_{i,j,k})$ $i, j, k \in \{out, side, long\}$) of the projected one-dimensional coarse histograms can be calculated without having large statistics.

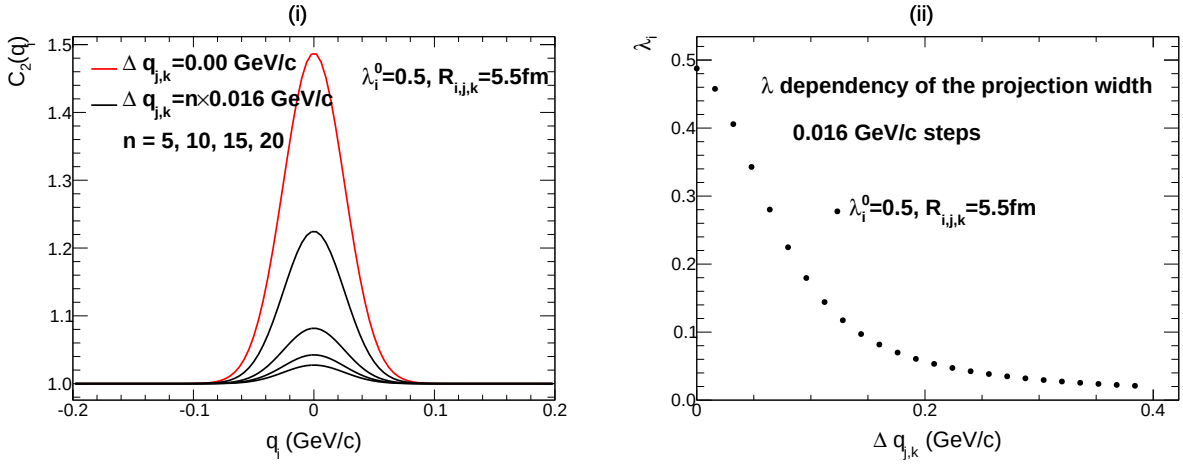

Figure 4.4.: (i) The fits of the two-photon correlation function for five different projection widths $\Delta q_{j,k} \in [0.0, 0.08, 0.16, 0.24, 0.32]$ GeV/c. (ii) As the projection width $\Delta q_{j,k}$ increases, the correlation strength λ_i of the projected momenta decreases. The shape of this dependency stays constant for all λ_i^0 and all projections.

The one-dimensional distributions of the relative momentum component q_i was calculated for different projection widths $\Delta q_{j,k} \in [0.0, 0.4]$ GeV/c. After projecting one axis q_i of the coarse background $B(\vec{q})$ and coarse signal histogram $A(\vec{q})$, the two-photon correlation function $C_2(q_i)$ of one component can be obtained by dividing the signal by the background:

$$C_2(q_i) = \frac{A(q_i)}{B(q_i)} \tag{4.2}$$

The results of the divisions are then be fitted by the one-dimensional functions of the two-photon correlation function given in expression 3.20:

$$C_2(q_i) = 1 + \lambda \cdot \exp\left(-q_i^2 R_i^2\right) \tag{4.3}$$

The input correlation strength for this analysis has been $\lambda^0 = 0.5$, while all three radii were set to $R_{i,j,k}$ =5.5 fm.

As shown in Figure 4.4 the amplitude, i.e. the correlation strength λ, of the fitted correlation functions decreases with increasing projection width $\Delta q_{j,k}$. As the projection width gets larger, a larger number of entries of the three-dimensional histogram are projected. The projection method integrates the values within the projection range. Hence, the amplitude of the single projections gets smaller. The shape of this dependency stays constant, no matter which input correlation strength λ^0 is used.

This has to be kept in mind when obtaining the projections of the three-dimensional two-photon correlation function for simulated HBT photons. In order to receive good fits of the projections, a sufficiently large number of photon pairs with relative momenta $(q_{out}, 0, 0)$, $(0, q_{side}, 0)$ and $(0, 0, q_{long})$ is required.
This is one reason of investigating the (averaged) one-dimensional parametrization of the correlation function $C_2(q_{inv})$ instead of the three-dimensional one.
However, the radius parameter of the projected correlation function seems to be independent of the projection width, wherefore it can be obtained if there is at least enough statistics to gain a fit of the projection.

4.1.3. Analysis of HBT Photons

In the first run the HBT signal has been investigated without adding any decay photons for both an average transverse momentum window of $0.10 < k_T < 0.20$ GeV/c and $0.20 < k_T < 0.30$ GeV/c. These ranges were chosen as the photon interferometry experiment reported by the WA98 collaboration utilized photon pairs of the same k_T windows.
Since the implemented algorithm makes use of the three-dimensional parametrization of the correlation function $C_2(\vec{q})$, an explicit analysis of the HBT photon generation will provide us with the input parameters R_{out}, R_{side} and R_{long} that we have to choose to obtain the invariant radii R_{inv} of the WA98 experiment.
For the transverse momentum windows $k_T \in (0.1, 0.2)$ GeV/c and $k_T \in (0.2, 0.3)$ GeV/c, the WA98 collaboration assigned values of R_{out} =5.0 fm, 5.5 fm and 5.1 fm for the R_{side} and 5.4 fm and 5.9 fm for the R_{long}, based on the values obtained from pion interferometry [17].
After running a simulation using some input values for R_{out}, R_{side} and R_{long}, the resulting HBT radii can be compared with the experimental results for each k_T bin. This way, one can check whether the performed assignment of the values obtained from pion interferometry is justified.
In order to simulate the probabilistic selection of photons, a sufficiently large number (2×10^7 events) of photons according to the thermal distribution was generated in a transverse momentum window $p_T \in [0.1, 2.5]$ GeV/c. This high number has been chosen to guarantee good statistics and to receive small statistical errors. Especially the error bars of the correlation function would be too high to gain reasonable fits, if $N_{ev.}$ is considerably smaller. The photons were randomly distributed uniformly over the azimuthal directions $\phi \in (-\pi, \pi)$ and the pseudo rapidity window $\eta \in (-0.9, 0.9)$. Next, photon

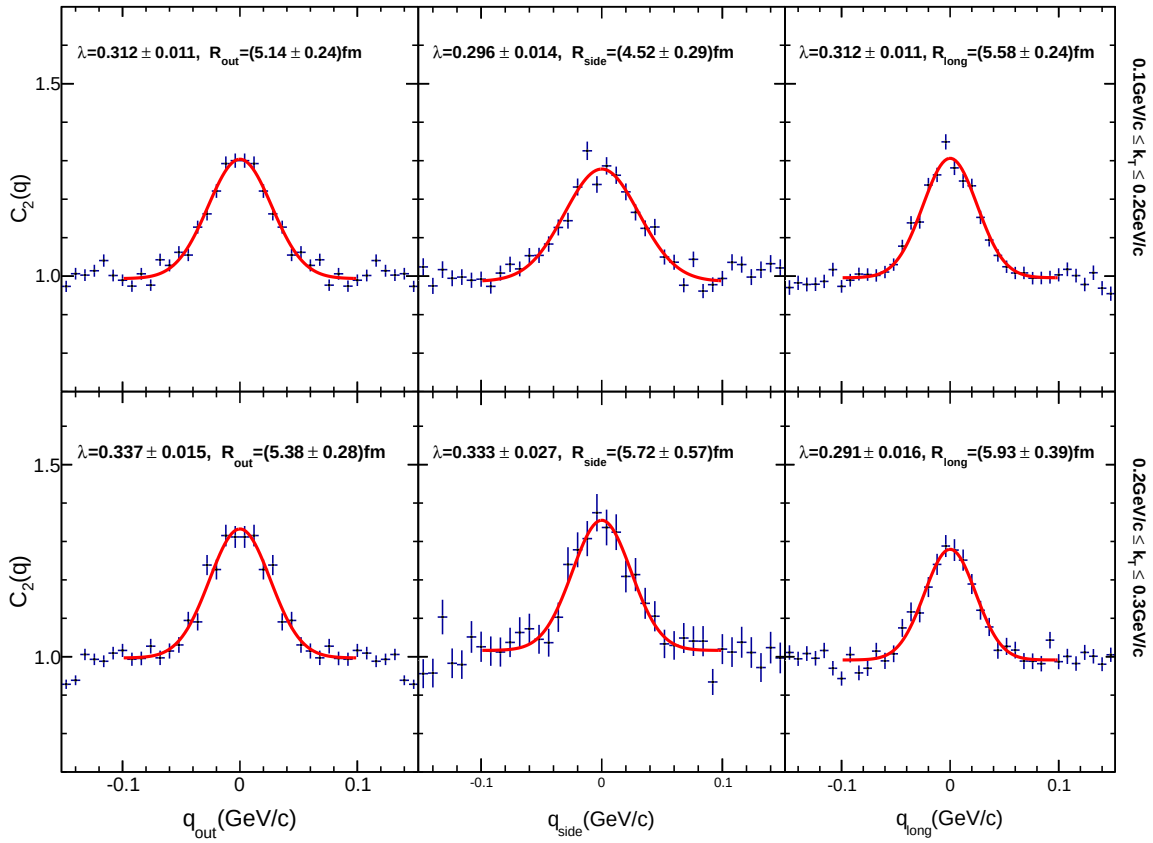

Figure 4.5.: Projections of the three-dimensional $\gamma\gamma$ correlation function (points) and the respective fits (lines), simulated in 2×10^7 events, $\eta < |0.9|$, $0.1 \leq p_T \leq 2.5$ GeV/c, $\lambda = 0.5$, $R_i = 5.5$ fm. When projecting on one axis, the other two components were required to be within $(-0.024, 0.024)$ GeV/c. The k_T range is indicated on the right-hand side axis.

pairs were sampled so that their average transverse momentum k_T was in the appropriate window. The correlation function was then calculated using expression 3.1. While the correlated numerator has been taking from photon pairs from the same event, the event mixing technique is applied to receive the uncorrelated denominator.

k_T [GeV/c]	R_{out} [fm]	R_{side} [fm]	R_{long} [fm]
$(0.1, 0.2)$	5.1 ± 0.2	4.5 ± 0.3	5.6 ± 0.2
$(0.2, 0.3)$	5.4 ± 0.3	5.7 ± 0.6	5.9 ± 0.4

Table 4.1.: Extracted radii R_{out}, R_{side} and R_{long} for two k_T bins.

Before analyzing the results for R_{inv}, we should have a look on the three-dimensional determination of the correlation function.

The input parameters of the radii were set to $R_{out} = R_{side} = R_{long}$ =5.5 fm for an overall transverse momentum range $k_T \in [0.1, 2.5]$ GeV/c.
To receive a significant statistic, the one-dimensional projections of the two-photon correlation function (see Figure 4.5) were generated within a projection width of $\Delta q_{j,k}$ =0.048 GeV/c.
The results of the three-dimensional determination of the correlation radii are listed in Table 4.1.

The reconstructed radii were found to differ slightly from the ones obtained from pion interferometry by up to 10%, depending on the component and k_T.
Since the projection width was chosen to be $\Delta q_{j,k}$ =0.048 GeV/c, the obtained correlation strengths λ cannot reach the input parameter 0.5. As shown in Figure 4.4(ii), a maximal correlation strength of $\lambda \cong 0.3$ is expected for this projection width. The obtained results are in good agreement with the expected ones.

Let us now have a look at the results for the one-dimensional correlation function in terms of the invariant momentum difference q_{inv}. As shown in Figure 4.6 the results are described to a reasonable accuracy by the form:

$$C_2(q_{inv}) = 1 + \lambda \cdot \exp\left(-R_{inv}^2 q_{inv}^2\right)$$

where $R_{inv} = (5.12 \pm 0.14)$fm and $\lambda = 0.31 \pm 0.01$ for the transverse momentum window $0.10 < k_T < 0.20$ GeV/c and R_{inv} =(5.93 ± 0.21) fm and $\lambda = 0.19 \pm 0.01$ for the transverse momentum window $0.20 < k_T$ <0.30 GeV/c.

However, there are some deviations of the fit for q_{inv} <0.01 GeV/c. The two-photon correlation function $C_2(q_{inv})$ gets calculated by division of a correlated signal histogram by an uncorrelated background histogram. In the lower q_{inv} domain both the signal and the background gets very small, thus the signal bins are divided by very small numbers and deviations from the theoretical correlation function are more pronounced in this region. Another explanation of this deviation is given by the fact, that the simulation accounts for momentum smearing due to Bremsstrahlung of the converted electrons.

The corresponding experimental results for R_{inv} obtained by the WA98 experiment are (5.4 ± 1.7) fm and (5.8 ± 2.0) fm, respectively.
The predictions of R_{inv} are in reasonable agreement with the experimental findings (within the errors).
Thus, the assignment of the radius parameters obtained from pion interferometry as it has been done in the WA98 experiment are a justified assumption and can be adopted to direct photon interferometry.
As the obtained results fit the experimental ones quite well, the overall input parameters $R_{out} = R_{side} = R_{long}$ =5.5 fm are retained unchanged for further investigations.
Since no decay photons were added yet, the obtained values of λ cannot be compared. However, the one-dimensional two-photon correlation function $C_2(q_{inv})$ approves the

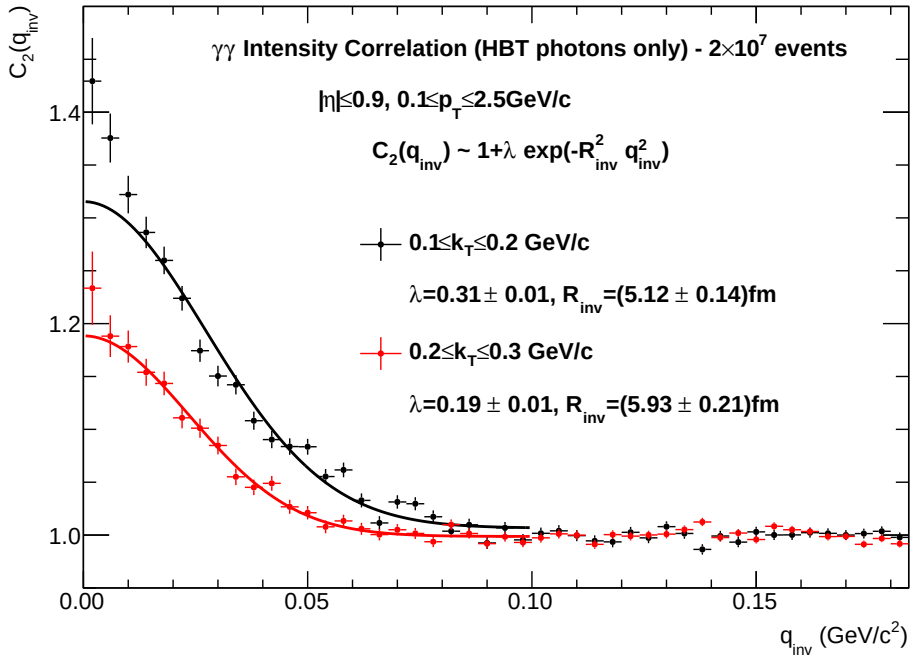

Figure 4.6.: The one-dimensional two-photon correlation function $C_2(q_{inv})$ for the average transverse momentum windows of $k_T \in (0.1, 0.2)$ GeV/c and $k_T \in (0.2, 0.3)$ GeV/c, assuming a fully chaotic source. Simulated in 2×10^7 events within the kinematic windows of $p_T \in [0.1, 2.5]$ GeV/c, $\eta \in (-0.9, 0.9)$ and $\phi \in (-\pi, \pi)$.

forecast that the effective correlation strength is considerably smaller than 1/2, even if there were no decay photons. This effect occurs, when we average over different projections of relative momentum, producing the same q_{inv}.
Obviously, the correlation strength decreases with k_T. Equation 3.22 of the invariant relative momentum q_{inv} can be rewritten in terms of η_i, ϕ_i and p_{T_i} of the two photons ($i \in \{1, 2\}$) [18]:

$$q_{inv} = \sqrt{2 p_{T_1} p_{T_2} \left[\cosh(\eta_1 - \eta_2) - \cos(\phi_1 - \phi_2)\right]} \tag{4.4}$$

As $q_{inv} \propto \sqrt{p_{T_i}}$, small values for q_{inv} can be obtained only if p_{T_i} are quite small. For larger values of p_{T_i}, the necessary η and ϕ bins would be too small to admit meaningful statistics. Thus it is no wonder that the WA98 experiment utilized only photon pairs having very low k_T.

4.2. Adding Decay Photons

The following sections present the obtained two-photon correlation functions after adding decay photons originated from $\pi^0 \rightarrow \gamma\gamma$ decays, which are the primary source of decay photons with a typically amount of $\approx$ 90% [8]. Other sources, including the decay of the η $(5 - 10\%)$ and $\eta\prime$ and ω (on the order of 1% each) are neglected within this simulation. A reasonable estimate of the significance of HBT correlations can be received by accounting only for the π^0 decay photons.
The simulation also considers various detector and photon reconstruction properties, which are explained briefly. A run of the simulation of direct photon HBT correlations plus π^0 decay photons has been performed with and without some of these properties. Thereby, the impact of the single detector properties on the HBT significance can be analyzed. The results of these investigations are presented within a one-dimensional analysis of the two-photon correlation function $C_2(q_{inv})$. Moreover, the final results are compared with the experimental ones obtained in the WA98 experiment.

4.2.1. Experimental Technique

One method of reconstructing π^0s is by detecting the photons of their primary decay $\pi^0 \rightarrow \gamma\gamma$ (with a branching ratio of $\cong$ 98.8% [32]) via Photon Conversion:

$$\pi^0 \rightarrow \gamma\gamma \rightarrow e^+e^-e^+e^- \tag{4.5}$$

The converted photons can be reconstructed by the Central Tracking System of ALICE. Photon pairs with a (combined) p_T are binned in pair invariant mass $m_{\gamma\gamma}$, which equals the invariant relative momentum q_{inv} in the case of massless particles, and the π^0s appear as a peak at $m_{\gamma\gamma} = q_{inv} = m_{\pi^0} \approx$0.135 GeV/$c^2$ on top of the combinatorial background.

In the MC simulation the π^0 decay photons are added by making use of the `PYTHIA6` [34] decayer class while having regard of the following constraints:

The geometrical acceptance of the detector is again given by the pseudo-rapidity range, wherefore only photons with $|\eta| < 0.9$ can be reconstructed. Since the reconstructed π^0s of the MC decayer appear as a δ-function, the peak is smeared to account for Bremsstrahlung of the electrons according to a certain function, which has been adapted from real data plots.

High energy photons lose energy in the detector material that leads to a low conversion probability $P_{conv.}$, which is defined as the fraction of converted to all generated photons $P^{\gamma}_{conv.} = N^{\gamma}_{conv.}/N^{\gamma}_{tot.}$. Within the pseudo-rapidity range of $|\eta| < 0.9$, $P^{\gamma}_{conv.}$ is about $\cong$ 8% [33], integrated from the vertex to the middle of the TPC. Although there is a drop in

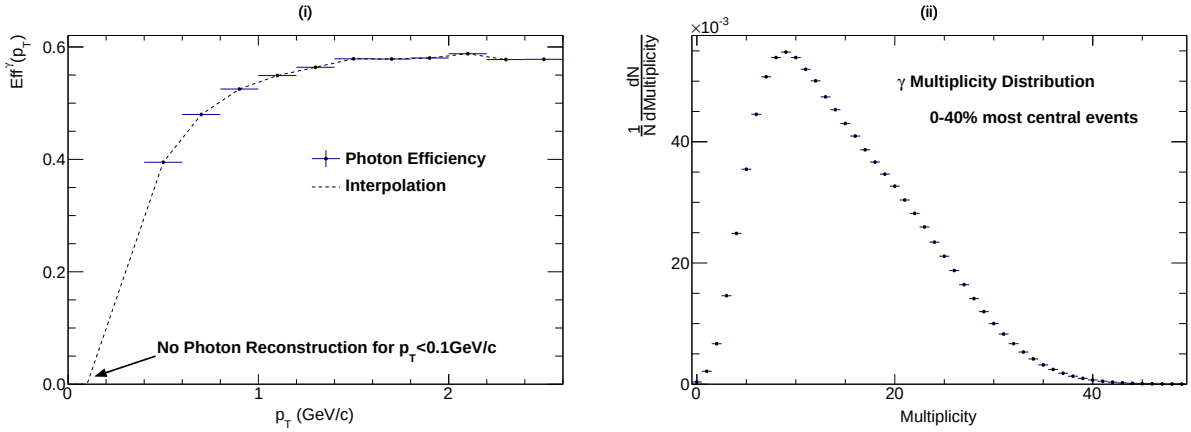

Figure 4.7.: (i) The efficiency to reconstruct a photon depends on its transverse momentum p_T. To account for the photon efficiency in the simulation, efficiency measurements observed in real data were interpolated. No photons can be reconstructed for p_T <0.1 GeV/c. (ii) As the γ multiplicity for the $0-40\%$ most central events is not constant, it gets picked randomly out of a distribution, which has been obtained in real data.

the conversion probability towards low transverse momenta this simulation assumes a constant conversion probability of $P^{\gamma}_{conv.} = 8\%$.
In order to reduce the runtime of the simulation, the case that both photons originated from a π^0 cannot be reconstructed is neglected so that at least one photon is reconstructed. While the conversion probability is applied for the decay photons, it is also assumed that two direct HBT photons are converted per event.

Figure 4.7(i) shows the reconstruction efficiency $\epsilon^{\gamma}_{reco.}$ for the photon candidates at $\sqrt{s}$ =2.76 TeV within $|\eta| < 0.9$ as a function of transverse momentum p_T. Due to the strength of the magnetic fields in the detector, the e^+ and e^- originated from photons with p_T <0.1 GeV/c have a very small radius of curvature, thus they are curling up and cannot be reconstructed anymore. Since photons convert under a certain energy asymmetry, it is possible, that the electron (positron) receives the main fraction of the γ energy, while the energy of the positron (electron) is too small to be reconstructible. This effect decreases with higher p_T, thus the photon reconstruction efficiency increases and reaches its maximum of $\cong 60\%$ for transverse momenta p_T >1.5 GeV/c.
To account for $\epsilon^{\gamma}_{reco.}$ the data points of the histogram shown in Figure 4.7(i) are interpolated, starting from p_T =0.1 GeV/c.

Another property that we have to account for is the non-constant photon multiplicity, i.e. the number of photons per event. Therefore the γ multiplicity gets picked randomly out of a distribution (see Figure 4.7(ii)), which has been obtained in the $0-40\%$ most central events of central Pb+Pb collisions at $\sqrt{s}$ =2.76 TeV within a pseudo-rapidity window of $|\eta| < 0.75$.

4.2.2. One dimensional Analysis

The one-dimensional two-photon correlation function $C_2(q_{inv})$ has been analyzed after decay photons were added to the MC simulation for both an average transverse momentum window of $0.10 < k_T < 0.20$ GeV/c and $0.20 < k_T < 0.30$ GeV/c. The measurement has been repeated under consideration of different detector and photon reconstruction properties.
In order to compare the results of the different measurements, the following input parameters of the simulation stayed constant:

- To gain sufficient statistics, a total number of $N_{ev.} = 2 \times 10^7$ events were simulated . Although the WA98 collaboration investigated a total sample of only 5.8×10^6 events [1], I adhered to a higher number of events to reduce statistical errors.
- The simulation considers the **special case** that exactly two direct photons are detected each event:
$$\frac{N^{\gamma}_{direct}}{N_{ev.}} = 2 \tag{4.6}$$
Thus, the simulation does not account for photon conversion probability in the case of direct photons.
- All photons (direct and decay photons) are generated within a transverse momentum window $p_T \in [0.1, 2.5]$ GeV/c, a pseudo-rapidity window $|\eta| < 0.9$ and azimuthal directions $\phi \in (-\pi, \pi)$.
While the direct photons follow the distributions described in 4.1.1 (1. Initialize Thermal Photon Generator), the decay photons are generated with the `PYTHIA6` decayer class of `AliRoot`.
- Photons are not reconstructed if their transverse momentum is below 0.1 GeV/c or their pseudo-rapidity exceeds $|\eta| > 0.9$.
- The three-dimensional coarse background histogram of the correlated photons is generated with a total number of 10^{10} entries.
- A fully chaotic source of direct photons is assumed, thus the input correlation strength was set to $\lambda = 1/2$. The input HBT radii for the theoretical three-dimensional two-photon correlation function $C_2(\vec{q})$ were $R_{out} = R_{side} = R_{long}$ =5.5 fm. This assignment has been turned out to provide results of the invariant Radius R_{inv} which are in good agreement with the ones obtained in the WA98 experiment (compare section 4.1.3).

The two photon correlation function $C_2(q_{inv})$ was calculated for both bins of k_T as the ratio of the photon pair invariant relative momentum q_{inv} where both photons are taken from the same event, to the same distribution but with photon pairs taken from different events. The ratio is normalized in the invariant relative momentum region of $q_{inv} > 0.15$ GeV/c, where neither the HBT signal is located nor the π^0 peak.

Constant γ-Multiplicity, No Photon Efficiency for Direct Photons

At first a constant decay photon multiplicity of $N^{\gamma}_{decay}/N_{ev.} = 20$ is assumed. Thereby the fraction of direct photons is approximately:

$$\frac{N^{\gamma}_{direct}}{N^{\gamma}_{tot.}} = \frac{N^{\gamma}_{direct}}{N^{\gamma}_{decay} + N^{\gamma}_{direct}} = \frac{2}{22} \approx 9\% \tag{4.7}$$

which is a reasonable estimate of the expected fraction of direct photons.
While the photon reconstruction efficiency $\epsilon^{\gamma}_{reco.}$ has been applied for the π^0 decay photons to simulate a realistic fraction of decay photons, no restrictions were made for the direct ones. This way the influence of the huge background due to the decay photons on the pure HBT signal can be studied. Additionally the relation of λ and the fraction of direct photons (equation 3.10) can be verified.

Figure 4.8 shows the resulting one-dimensional two-photon correlation functions with (left hand side) and without (right hand side) consideration of the π^0 decay photons. Both the correlation strength λ and the invariant radius parameter R_{inv} were extracted from a fit of the one-dimensional parametrization of $C_2(q_{inv})$ and are listed in Table 4.2.

Scenario	k_T [GeV/c]	R_{inv} [fm]	λ	$\sqrt{2\lambda} = N^{\gamma}_{direct}/N^{\gamma}_{tot.}$
HBT only	$(0.1, 0.2)$	5.2 ± 0.1	0.34 ± 0.01	-
	$(0.2, 0.3)$	6.1 ± 0.2	0.21 ± 0.01	-
HBT+Decay	$(0.1, 0.2)$	4.9 ± 1.0	$(4.4 \pm 0.7) \times 10^{-3}$	$(9 \pm 3)\%$
	$(0.2, 0.3)$	6.6 ± 1.0	$(5.9 \pm 1.2) \times 10^{-3}$	$(11 \pm 5)\%$

Table 4.2.: Extracted invariant radii R_{inv} and correlation strengths λ for two k_T bins with and without adding π^0 decay photons.

The values for R_{inv} for the scenario without consideration of the decay photons are in good agreement with the ones obtained in the analysis of HBT Photons in section 4.1.3 (within the errors), which were (5.1 ± 0.1) fm for the transverse momentum window $0.10 < k_T < 0.20$ GeV/c and $(5.9 \pm 0.2) \pm$ fm for the transverse momentum window $0.20 < k_T < 0.30$ GeV/c. Also both values for λ conform within the errors ($\lambda = 0.31 \pm 0.01$ and $\lambda = 0.19 \pm 0.01$ for the respective k_T windows).
When analyzing the corresponding correlation functions under consideration of the π^0 decay photons (see Figure 4.2, right hand side) it is apparent that the extracted correlation strength drops dramatically from $\lambda = 0.33 \pm 0.01$ and $\lambda = 0.21 \pm 0.01$ to values of the magnitude of $\cong 5 \times 10^{-3}$. After adding decay photons, the overall spectrum of q_{inv} is composed of a large number of photon pairs where at least one photon is not a direct one. These photon pairs superimpose the HBT signal both in the signal histogram and the (mixed events) background histogram, thus the correlation strength decreases.

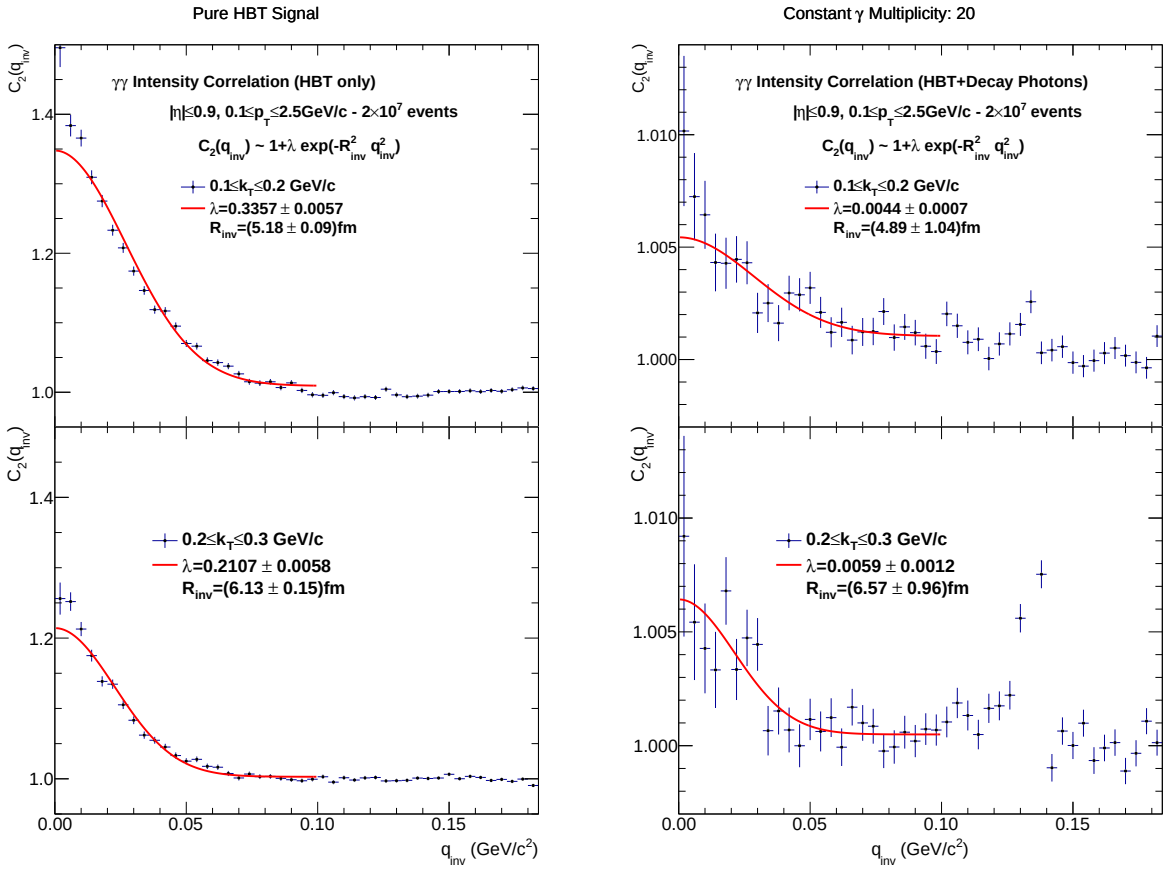

Figure 4.8.: The one-dimensional two-photon correlation function $C_2(q_{inv})$ for both the average transverse momenta $k_T \in (0.1, 0.2)$ GeV/c and $k_T \in (0.2, 0.3)$ GeV/c with (left) and without (right) π^0 decay photons. While a constant γ multiplicity of 20 was considered, the photon efficiency $\epsilon^{\gamma}_{reco.}$ was not applied for the direct photons. The correlation strength λ and the invariant Radii R_{inv} are obtained by fits (red lines) of the one-dimensional parametrization of $C_2(q_{inv})$.

The fraction of direct photons can be calculated according to equation 3.10. Under the assumption of a fully chaotic direct photon source $N^{\gamma}_{direct}/N^{\gamma}_{total}$ can be obtained by calculating $\sqrt{2\lambda}$. As listed in Table 4.2, the obtained fractions are $\cong$ 9% for the first transverse momentum window $k_T \in (0.1, 0.2)$ GeV/c and $\cong$ 11% respectively for $k_T \in (0.2, 0.3)$ GeV/c, which are in good agreement with the fraction of photons which has been put into ($\cong$ 9%).
Contrary to λ, the invariant radius parameter stays roughly constant with and without decay photons. The extracted R_{inv} comply within 1σ. However, the statistical errors increase in the case of considering direct plus decay photons because the histograms are fitted within a range where the statistical error of each bin is large compared to the

corresponding value of $C_2(q_{inv})$.
While the π^0 peak at $q_{inv} \cong 0.135$ GeV/c^2 is significant in the average transverse momentum of $0.20 < k_T < 0.30$ GeV/c, it is vaguely perceptible for $0.10 < k_T < 0.20$ GeV/c. In this momentum region the reconstruction efficiency is too low to provide a significant π^0 signal.

Non-constant γ Multiplicity and Photon Reconstruction Efficiency for HBT Photons

In the next step the simulation of direct photons plus decay photons originated from π^0 decays is approximated progressively to an experimental environment.
To account for a non-constant decay photon multiplicity the γ multiplicity distribution of Figure 4.7(ii) was implemented. The multiplicity of the decay photons are then picked randomly out of this distribution for each event.
Again the two-photon correlation function $C_2(q_{inv})$ is calculated for the k_T bins $(0.1, 0.2)$ GeV/c and $(0.1, 0.2)$ GeV/c. The extracted HBT parameters can then be compared to the obtained results of the above analysis when a constant γ multiplicity of 20 was assumed.
This has been done in a first simulation, where again the photon reconstruction efficiency $\epsilon^{\gamma}_{reco.}$ shown in Figure 4.7(i) has been applied only for the π^0 decay photons.
Additionally a second simulation ran where $\epsilon^{\gamma}_{reco.}$ has been applied both for the π^0 decay photons and the direct photons. To account for the reconstruction efficiency, the thermal p_T spectrum of the direct photon generator was multiplied by the interpolated $\epsilon^{\gamma}_{reco.}$ histogram. This way the influence of $\epsilon^{\gamma}_{reco.}$ on the HBT signal can be studied explicitly for the case of a non-constant γ multiplicity.

The two-photon correlation functions $C_2(q_{inv})$ of both simulations are presented in Figure 4.9, where the results of the first simulation (regardless of $\epsilon^{\gamma}_{reco.}$ for the HBT photons) are shown on the left hand side. The obtained correlation functions having regard to $\epsilon^{\gamma}_{reco.}$ for the direct photons can be seen on the right hand side.
Again the HBT parameters were extracted from a fit of the one-dimensional parametrization of $C_2(q_{inv})$:

Scenario	k_T [GeV/c]	R_{inv} [fm]	λ	$\sqrt{2\lambda}$
$\epsilon^{\gamma}_{reco.}$ for HBT photons OFF	$(0.1, 0.2)$	5.6 ± 0.8	$(10.0 \pm 1.5) \times 10^{-3}$	$(14 \pm 5)\%$
	$(0.2, 0.3)$	4.9 ± 0.7	$(10.5 \pm 1.5) \times 10^{-3}$	$(14 \pm 5)\%$
$\epsilon^{\gamma}_{reco.}$ for HBT photons ON	$(0.1, 0.2)$	4.3 ± 1.4	$(2.4 \pm 1.1) \times 10^{-3}$	$(7 \pm 5)\%$
	$(0.2, 0.3)$	10.8 ± 6.2	$(3.1 \pm 3.1) \times 10^{-3}$	$(8 \pm 8)\%$

Table 4.3.: Extracted invariant radii R_{inv} and correlation strengths λ for the two k_T bins when a non-constant γ multiplicity was considered.

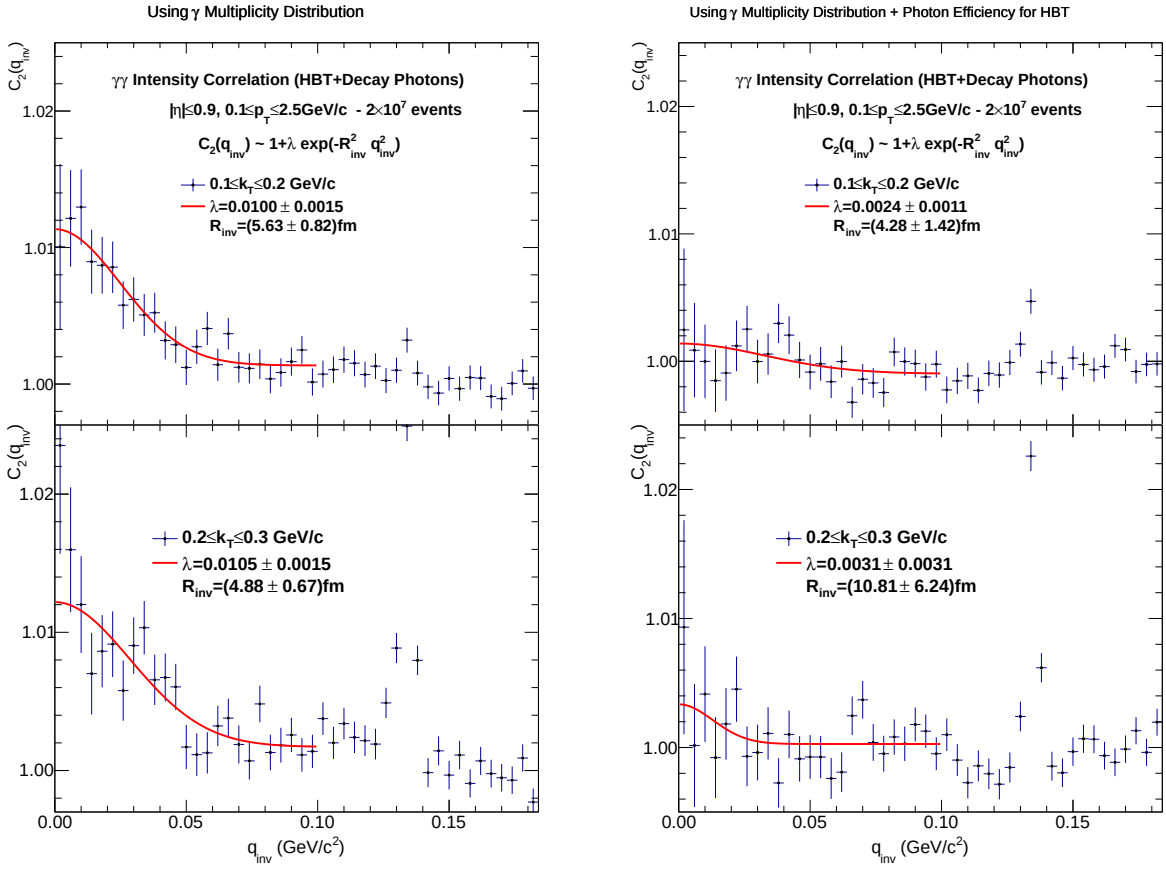

Figure 4.9.: Obtained two-photon correlation functions $C_2(q_{inv})$ for both the average transverse momenta $k_T \in (0.1, 0.2)$ GeV/c and $k_T \in (0.2, 0.3)$ GeV/c under consideration of a non-constant γ multiplicity, with (left) and without (right) accounting for the photon reconstruction efficiency $\epsilon^{\gamma}_{reco.}$ for the direct photons.

Let us first have a look on the results without accounting for $\epsilon^{\gamma}_{reco.}$ for the direct photons (Scenario: $\epsilon^{\gamma}_{reco.}$ for HBT photons OFF). The obtained values for R_{inv} agree with the corresponding radii obtained in the former analyses within 1σ. This observation leads to the declarative statement that the invariant radii seem to be quite robust, no matter which fraction of direct photons is put into.
Compared to the extracted correlation strengths λ obtained under the consideration of a constant γ multiplicity of 20 (see Table 4.2), the extracted values of λ increased by a factor of $\cong 2$.
To study this rise we have to look at the γ multiplicity distribution (Figure 4.7(ii)). The mean of the distribution is approximately $\cong 15$. Thus, the input fraction of direct photons can be estimated to $N^{\gamma}_{direct}/N^{\gamma}_{total} = 2/17 \cong 12\%$.
Whilst taking into account this estimate, the obtained results for $\sqrt{2\lambda}$ coincide within

their errors for both the average transverse momentum windows $0.1 < k_T < 0.2$ GeV/c and $0.2 < k_T < 0.3$ GeV/c.

As opposed to this, the second scenario where the simulation accounts for $\epsilon^{\gamma}_{reco.}$ for both the decay photons **and** the direct photons, no significant HBT signal can be registered in the low q_{inv} region. In this case the transverse momenta p_T of the direct photons gets randomized out of the product of a thermal p_T spectrum and $\epsilon^{\gamma}_{reco.}$. Since $\epsilon^{\gamma}_{reco.}$ is of the order of $\cong 2 \times 10^{-1}$ in the p_T window of $0.1 < p_T < 0.3$ GeV/c, the probability of generating photons with transverse momenta $p_T < 0.3$ GeV/c decreases, while higher p_T are getting more likely. These higher p_T photons do not contribute in the q_{inv} spectrum of the investigated k_T bins. Therefore the statistical errors of the q_{inv} distribution increase and the performed fits of $C_2(q_{inv})$ do not describe the correlation functions to a reasonable accuracy.
In spite of that the extracted fractions of direct photons $\sqrt{2\lambda} = N^{\gamma}_{direct}/N^{\gamma}_{total}$ are in agreement with the expected value of $\cong$ 12% (within their errors) for both k_T bins. While the invariant radius R_{inv} of a k_T window of $(0.1, 0.2)$ GeV/c provides a result that complies with the ones obtained in the previous analyses, the extracted R_{inv} of the k_T window of $(0.2, 0.3)$ GeV/c is about 2 times larger than expected ($\cong$5.5 fm) and suffers a large statistical error of ΔR_{inv} =6.2 fm.

All in all it can be noted that no significant HBT signal can be observed for a total number of 2×10^7 events if we consider the photon reconstruction efficiency for all photons (decay photons and direct photons). If the reconstruction efficiency would be higher, especially for low transverse momenta $p_T < 0.3$ GeV/c, a way more significant signal would be observable. This can be seen particularly in the first simulations where the photon efficiency was omitted.

4.2.3. Comparison to WA98 results

All simulations were performed in that manner that the invariant radii R_{inv} agree with the ones determined by the WA98 collaboration.
In order to cross-check the simulation the extracted R_{inv}, can be compared to the experimental results. The relative deviation of R_{inv} is given by:

$$\frac{\delta R_{inv}}{R_{inv}^{WA98}} = \left| 1 - \frac{R_{inv}}{R_{inv}^{WA98}} \right| \tag{4.8}$$

Table 4.4 summarizes the results of the three different MC simulations and lists the deviations of R_{inv}.

Scenario	k_T [GeV/c]	R_{inv} [fm]	$\delta R_{inv}/R_{inv}^{WA98}$
WA98	$(0.1, 0.2)$	5.4 ± 1.7	-
	$(0.2, 0.3)$	5.8 ± 2.0	-
Const. Multiplicity (20), $\epsilon_{reco.}^{HBT}$ OFF	$(0.1, 0.2)$	4.9 ± 1.0	9% (1σ)
	$(0.2, 0.3)$	6.6 ± 1.0	14% (1σ)
Non-Const. Multiplicity, $\epsilon_{reco.}^{HBT}$ OFF	$(0.1, 0.2)$	5.6 ± 0.8	4% (1σ)
	$(0.2, 0.3)$	4.9 ± 0.7	16% (1σ)
Non-Const. Multiplicity, $\epsilon_{reco.}^{HBT}$ ON	$(0.1, 0.2$	4.3 ± 1.4	20% (1σ)
	$(0.2, 0.3)$	10.8 ± 6.2	86% (1σ)

Table 4.4.: Extracted HBT parameters of the WA98 experiment and three MC simulations after adding π^0 decay photons where different γ reconstruction constraints and γ multiplicities were used.

The term $\epsilon_{reco.}^{HBT}$ (ON) means that the respective simulation has been performed under consideration of the photon reconstruction efficiency for the direct photons ($\epsilon_{reco.}^{HBT}$ OFF if not).
The R_{inv} are in a 1σ agreement with the experimental results for both k_T bins and simulations. This approves the observation that R_{inv} is mostly independent of the fraction of direct photons to the total number of photons. Though, the deviation for the average transverse momentum window of $0.2 < k_T < 0.3$ GeV/c of the last simulation where the HBT signal is not significant and no reasonable fit of the correlation function has been achieved rises up to 86%.

4.2.4. Significance of the HBT signal

Table 4.5 summarizes the extracted fractions of direct photons $\sqrt{2\lambda} = N_{dir.}^{\gamma}/N_{tot.}^{\gamma}$ and compares them with the fraction that is put into for each performed MC simulation. The significance of an HBT signal is given by the correlation strength λ.

Scenario	k_T [GeV/c]	λ [$\times 10^{-3}$]	$\sqrt{2\lambda}$	$(N^{\gamma}_{dir.}/N^{\gamma}_{tot.})_{Input}$
Const. Mult. (20), $\epsilon^{HBT}_{reco.}$ OFF	$(0.1, 0.2)$	4.4 ± 0.7	$(9 \pm 3)\%$	9%
	$(0.2, 0.3)$	5.9 ± 1.2	$(11 \pm 5)\%$	
Non-Const. Mult., $\epsilon^{HBT}_{reco.}$ OFF	$(0.1, 0.2)$	10.0 ± 1.5	$(14 \pm 5)\%$	$\cong 12\%$
	$(0.2, 0.3)$	10.5 ± 1.5	$(14 \pm 5)\%$	
Non-Const. Mult., $\epsilon^{HBT}_{reco.}$ ON	$(0.1, 0.2)$	2.4 ± 1.1	$(7 \pm 5)\%$	$\cong 12\%$
	$(0.2, 0.3)$	3.1 ± 3.1	$(8 \pm 8)\%$	

Table 4.5.: Extracted fractions of direct photons for all different MC simulations The significance of the HBT signal is given by the correlation strength λ.

Under the hypothesis that an HBT signal is measured if $\lambda > 0$ and no HBT signal is measured if $\lambda = 0$, the single scenarios can be compared.
Significant HBT signals can be observed when we do not account for the photon efficiency for the direct photons ($\epsilon^{HBT}_{reco.}$ OFF). Having regard to the corresponding errors, the extracted values for λ are substantially larger than 0 and the calculated fraction of direct photons agrees with the input fraction within 1σ.
Indeed, the 1σ deviation of the calculated fraction of direct photons holds also for the last scenario where the photon efficiency for the direct photons is considered ($\epsilon^{HBT}_{reco.}$ ON), but the corresponding values of λ are no longer significant, especially for the average transverse momentum range $0.2 < k_T < 0.3$ GeV/c where $\lambda = (3.1 \pm 3.1) \times 10^{-3}$.
The huge background due to π^0 decay photons is the main reason of not gaining a significant fit of the correlation function. Obviously the background becomes a larger influence in the case when we additionally account for the γ reconstruction efficiency for the direct photons. Here, the thermal transverse momentum spectrum whence the direct photons are picked is multiplied with the γ reconstruction efficiency distribution and the probability of picking photons with small transverse momenta (p_T <0.5 GeV/c) decreases dramatically.
As the invariant pair relative momentum $q_{inv} \propto p_{T_i}$ (compare eq. 4.4) of the single photons of the pair, a rise of small values for q_{inv} can only be observed if p_{T_i} are quite small. Thus, no significant HBT signal can be observed if we additionally determine the correlation function for k_T >0.3 GeV/c.

Chapter 5.

Conclusion

5.1. Summary of the Results

Within this thesis the feasibility to observe a significant signal of direct photon correlations with the ALICE detector was studied. For this purpose an algorithm has been developed that is able to simulate HBT correlations of direct photons originated from a static thermal source. There is no other generator of HBT correlations yet implemented in the `AliRoot` framework that provides reasonable results for photons. In order to reduce the complexity of such a simulation the special case of emitting and detecting two correlated direct photons per event has been considered. The developed algorithm makes use of a three-dimensional parametrization of the two-photon correlation function. Thus, it is possible to study both the three-dimensional and the one-dimensional determination of the correlation function in an elegant manner.

Section 4.1.2 demonstrates that if one is interested in a projection of the three-dimensional correlation function ($C_2(q_{out})$, $C_2(q_{side})$ or $C_2(q_{long})$) the used projection width of the others plays a major role. While the extracted radii R_{out}, R_{side} and R_{long} are mostly independent of the projection width, λ is highly correlated to the projection width.

In an explicit analysis of HBT correlations of direct photons (without adding any decay photons) the simulation was performed in this manner that the invariant radii R_{inv} approximately match the ones of the WA98 experiment. Thereby the corresponding values of R_{out}, R_{side} and R_{long} for R_{inv} were obtained for both k_T bins. It has been shown in 4.1.3 that the assignment of three-dimensional radius parameters obtained by pion interferometry as it has been done in the WA98 experiment is a justified assumption and can be adopted to direct photons.

In order to account for the huge background due to decay photons, photons originated from neutral $\pi^0 \rightarrow \gamma\gamma$ decays were added to the simulation. The one-dimensional correlation function $C_2(q_{inv})$ was determined for both the transverse momentum windows $0.1 < k_T < 0.2$ GeV/c and $0.2 < k_T < 0.3$ GeV/c within a total number of 2×10^7 events. Step by step various effects like a non-constant multiplicity of π^0 decay photons and the photon reconstruction efficiency have been implemented into the simulation. After

adding the π^0 decay photons the obtained correlation strength decreases dramatically to values of the order of $\cong 5 \times 10^{-3}$. Under the assumption of a fully chaotic source the fraction of direct photons $N^{\gamma}_{direct}/N^{\gamma}_{total}$ can be estimated by calculating $\sqrt{2\lambda}$. This relation even holds after we additionally account for a non-constant γ multiplicity and the photon reconstruction efficiency for the direct photons.

However, no significant HBT signal is observable when we account for the photon reconstruction efficiency both for the decay photons and the direct photons. The correlation strengths were determined to $\lambda = (2.4 \pm 1.1) \times 10^{-3}$ for an average transverse momentum window $k_T \in (0.1, 0.2)$ GeV/c and $\lambda = (3.1 \pm 3.1) \times 10^{-3}$ for $k_T \in (0.2, 0.3)$ GeV/c, respectively.
Since the direct photons are generated by randomizing out of a p_T distribution which is composed of the product of the photon reconstruction efficiency and a thermal p_T spectrum, photons with p_T >0.5 GeV/c are getting more likely. These higher p_T photons do not contribute in the q_{inv} spectrum of the investigated k_T bins. Therefore the statistical errors of the q_{inv} distribution increase and the performed fits of $C_2(q_{inv})$ do not describe the correlation functions to a reasonable accuracy.

Additionally it has to be noted that the combination of so-called fake tracks also are able to give rise to low invariant masses ($m_{\gamma\gamma} < 0.05$ GeV/c^2) in the π^0 spectrum [41]. Fake tracks occur due to faulty track reconstructions of the used reconstruction algorithms. A large number of fake tracks is expected to appear in regions where the track density is high, when the algorithm suffers bugs or the distance between the single track digits gets large. Before preparing an explicit measurement of photon-photon correlations this impact should be controlled.

5.2. Outlook

There are a few considerations which may lead to a more significant HBT signal. While the implemented thermal photon generator makes use of a temperature of T =0.266 GeV/c, latest results of the ALICE Photon Conversion Group rather assume a temperature of around T =0.300 GeV/c. Since T is the (inverse) slope of the thermal spectrum $dN/dp_T p_T \propto \exp(-p_T/T)$, a higher value of T increases the probability of picking photons with small p_T out of the distribution. Thus it is suitable to perform the simulation with this up-to-date number.
Moreover, the simulation only considers a special case that exactly two direct photons are emitted per event, while the fraction $N^{\gamma}_{direct}/N^{\gamma}_{total} \cong 10\%$. Assuming a higher number of this fraction, one way to achieve a more significant HBT signal would be to increase the number of thermal photons per event. Indeed, only two photons per event are correlated and the input correlation strength (i.e. the correlation strength when no decay photons are added) would decrease. But on the other hand a higher number of direct photons pairs with an average transverse momentum k_T <0.3 GeV/c would be generated. Thus, the statistical errors of the fits of $C_2(q_{inv})$ would decrease and more precise parameters

could be extracted.
When the simulation is performed with smaller decay photon multiplicities, the background due to decay photons would also lose influence on the q_{inv} spectrum. Thus, considering less central events (e.g. $20 - 40\%$ centrality class instead) are a worthwile measurement as well.

Appendix A.

Relativistic kinematic variables

Ultrarelativistic reactions are characterized by different kinematic variables.
In high energy physics particles are described by introducing the four momentum

$$p^\mu = (E, \vec{p}) = (E, p_x, p_y, p_z) \tag{A.1}$$

Here, E is the energy of the particle while $\vec{p}$ denotes its three momentum in cartesian coordinates. In this notation, natural units are used, i.e $c \equiv \hbar \equiv 1$. Free particles with a rest mass m_0 follow the relativistic energy momentum relation

$$E^2 = m_0^2 + \vec{p}^2 \tag{A.2}$$

The Lorentz invariant norm of the four momentum p^μ is called the invariant mass

$$m_{inv}^2 = p_\mu p^\mu = E^2 - \vec{p} \cdot \vec{p} \tag{A.3}$$

Since the z-axis of the coordinate system in accelerator physics is determined by the beam axis, the three momentum of a particle can be decomposed into a longitudinal momentum p_L and a transverse momentum p_T:

$$|\vec{p_L}| = |\vec{p}| \cdot \cos\theta = p_z \tag{A.4}$$

$$|\vec{p_T}| = |\vec{p}| \cdot \sin\theta = \sqrt{p_x^2 + p_y^2} \tag{A.5}$$

Here, θ denotes the angle of the propagation direction of the particle towards the beam axis, while $|\vec{p}|$ is the norm of the three momentum. Contrary to p_T, the longitudinal momentum component p_L is not Lorentz invariant. Hence, the longitudinal velocity $\beta_L = p_L/E$ of particles is typically described by the so called rapidity y of the boost along the beam axis which takes an observer from the lab frame to a frame in which particle moves only perpendicular to the beam:

$$y = \operatorname{atanh}(\beta_L) = \frac{1}{2} \ln \frac{E + |\vec{p_L}|}{E - |\vec{p_L}|} \tag{A.6}$$

For massless particles and highly relativistic particles, where $E \gg m_0$, the rapidity y can be approximated by the pseudorapidity η:

$$\eta = -\ln\left[\tan\left(\frac{\theta}{2}\right)\right] \tag{A.7}$$

where θ is the angle between the particle three momentum $\vec{p}$ and the beam axis.

Bibliography

[1] M.M. Aggarwal et al. Interferometry of direct photons in central Pb-208+Pb-208 collisions at 158-A-GeV. *Phys.Rev.Lett.*, 93:022301, 2004.

[2] CERN press office. http://static.ddmcdn.com/gif/large-hadron-collider-9.jpg.

[3] CERN press office. CERN experiments observe particle consistent with long-sought Higgs boson, http://press.web.cern.ch/press/PressReleases/Releases2012/PR17.12E.html.

[4] K. Werner. Quark-Gluon-Plasma Formation at CERN-SPS Energies (200 GeV). *Phys. Rev. Lett.*, 73:1594–1597, Sep 1994.

[5] K. Adcox et al. Formation of dense partonic matter in relativistic nucleus-nucleus collisions at RHIC: Experimental evaluation by the PHENIX collaboration. *Nucl.Phys.*, A757:184–283, 2005.

[6] S. Bathe. PHENIX Physics Highlights. *Quark Matter, Int. Conf. Ultra-Rel. Nucl.-Nucl. Coll.*, 2011.

[7] S. Afanasiev et al. Measurement of Direct Photons in Au+Au Collisions at $\sqrt{s_{NN}} =$ 200 GeV. 2012.

[8] P. Stankus. Direct photon production in relativistic heavy-ion collisions. *Ann.Rev.Nucl.Part.Sci.*, 55:517–554, 2005.

[9] M. Wilde *et. al.* Direct Photon Spectrum. *QM 2012*, 2012.

[10] (Ed.) Carminati, F et al. ALICE: Physics performance report, volume I. *J.Phys.G*, G30:1517–1763, 2004.

[11] (Ed.) Carminati, F et al. ALICE: Physics performance report, volume II. *J.Phys.G*, G30:1517–1763, 2004.

[12] U.Heinz U. Wiedemann. Particle interferometry for relativistic heavy-ion collisions. *Physics Reports*, 319:145 – 230, 1999.

[13] B.V. Jacak U.Heinz. Two-particle correlations in relativistic heavy-ion collisions. *Ann. Rev. Nucl. Part. Sci.*, 49:9902020, 1999.

[14] D. Peressounko. Hanbury Brown Twiss interferometry of direct photons in heavy ion collisions. *Phys.Rev.Lett.*, 67(1):014905, January 2003.

[15] U. Heinz C. Slotta. Photon spin and the shape of the two-photon correlation function. *Phys.Rev.Lett.*, pages 469–473, 1997.

[16] M. Sekora. The Big Bang's pervasive plasma: the Quark-Gluon Plasma. *MURJ*, 6:13, 2002.

[17] M.M. Aggarwal et al. One-, two-, and three-particle distributions from 158aGeV/c central pb+pb collisions. *Phys. Rev. C*, 67:014906, Jan 2003.

[18] D. K. Srivastava. Intensity interferometry of thermal photons from relativistic heavy-ion collisions. *Phys. Rev. C*, 71:034905, Mar 2005.

[19] D. Magestro. HBT: A (Mostly) experimental overview. *J.Phys.G*, G31:265–272, 2005.

[20] K. Aamodt et al. Two-pion Bose-Einstein correlations in central Pb-Pb collisions at $\sqrt{s_{NN}} = 2.76$ TeV. *Phys.Lett.*, B696:328–337, 2011.

[21] D. M. Reichhold. *Two-Kaon and Two-Proton Interferometry in 158GeV/Nucleon Pb+Pb Collisions*. PhD thesis, Ohio State University, 2001.

[22] G. Wilk. HBT Interferometry with Photons and Pions. *ALICE Internal Note*, 98-53, 1998.

[23] R. Hanbury Brown and R. Q. Twiss. A Test of a New Type of Stellar Interferometer on Sirius. *Nature*, 178:1046, 1956.

[24] R. Hanbury Brown and R. Q. Twiss. The Question of Correlation between Photons in Coherent Light Rays. *Nature*, 178:1447–1448, 1956.

[25] Lee W.-Y. Pais A. Goldhaber G., Goldhaber S. Influence of Bose-Einstein Statistics on the Antiproton-Proton Annihilation Process. *Phys. Rev. Letr.*, 120:300, 1960.

[26] Gordon Baym. The Physics of Hanbury Brown-Twiss intensity interferometry: From stars to nuclear collisions. *Acta Phys.Polon.*, B29:1839–1884, 1998.

[27] Heinz U. How to extract physics from HBT radius parameters. *Nucl. Phys. A*, 610:264c, 1996.

[28] Wiedemann U. A. Heinz U. Particle Interferometry for Relativistic Heavy-Ion Collisions. *Physics Reports*, 319:145–230, 1999.

[29] Y. Sinyukov. Hot Hadronic Matter: Theory and Experiment. *Nucl.Phys.A566*, 589c:309, 1994.

[30] S. V. Akkelin Y. Sinyukov. The HBT-interferometry of expanding sources. *Phys. Rev. Lett.*, B356:525, 1995.

[31] B. K. Jennings D. H. Boal, C. Gelbke. Intensity interferometry in subatomic physics. *Rev. Mod. Phys*, 64:553, 1990.

[32] K. Nakamura *et al.* (Particle Data Group). Particle physics booklet, July 20010.

[33] K. Koch. *Measurement of π^0 and η mesons with photon conversions in ALICE in proton-proton collisions at $\sqrt{s}$ = 0.9, 2.76, 7 TeV*. PhD thesis, University of Heidelberg, 2012.

[34] Torbjorn Sjostrand, Stephen Mrenna, and Peter Z. Skands. PYTHIA 6.4 Physics and Manual. *JHEP*, 0605:026, 2006.

[35] S.K. Kaufmann M. Gyulassy and L.W. Wilson. Pion interferometry of nuclear collisions. I. Theory. *Phys. Rev.*, C20:2267, 1979.

[36] S. Pratt. Pion Interferometry for Exploding Sources. *Phys.Rev.Lett.*, 53:1219–1221, 1984.

[37] S. Pratt. Pion Interferometry of Quark-Gluon Plasma. *Phys.Rev.*, D33:1314–1327, 1986.

[38] G. Bertsch, M. Gong, and M. Tohyama. Pion interferometry in ultrarelativistic heavy-ion collisions. *Phys. Rev. C*, 37:1896–1900, May 1988.

[39] Yu.M. Sinyukov. Hanbury Brown/Twiss Correlations for Expanding Hadron and Quark-Gluon Matter. *Nucl.Phys.*, A498:151C–160C, 1989.

[40] G. W. Hoffmann L. R. Ray. Simulation Method for Studying Bose-Einstein Correlations in Relativistic Heavy-Ion Collisions. *Phys.Rev*, C54:2582, 1996.

[41] D. Lohner. Private Communication, Fake Photons, 2012.

Erklärung

Ich versichere, dass ich diese Arbeit selbstständig verfasst und keine anderen als die angegebenen Quellen und Hilfsmittel benutzt habe.

Heidelberg, 06. August 2012 _____

Manuel Meske